

# Electromagnetically induced transparency in superconducting quantum circuits : Effects of decoherence, tunneling and multi-level cross-talk

Zachary Dutton<sup>1</sup>, K. V. R. M. Murali<sup>2</sup>, William D. Oliver<sup>3</sup>, and T. P. Orlando<sup>2</sup>

<sup>1</sup>*Naval Research Laboratory, Washington, DC 20375*

<sup>2</sup>*Department of Electrical Engineering and Computer Science  
Massachusetts Institute of Technology, Cambridge MA 02138*

<sup>3</sup>*MIT Lincoln Laboratory, 44 Wood Street, Lexington, MA 02420*

(Dated: January 1, 2022)

## Abstract

We explore theoretically electromagnetically-induced transparency (EIT) in a superconducting quantum circuit (SQC). The system is a persistent-current flux qubit biased in a  $\Lambda$  configuration. Previously [Phys. Rev. Lett. **93**, 087003 (2004)], we showed that an ideally-prepared EIT system provides a sensitive means to probe decoherence. Here, we extend this work by exploring the effects of imperfect dark-state preparation and specific decoherence mechanisms (population loss via tunneling, pure dephasing, and incoherent population exchange). We find an initial, rapid population loss from the  $\Lambda$  system for an imperfectly prepared dark state. This is followed by a slower population loss due to both the detuning of the microwave fields from the EIT resonance and the existing decoherence mechanisms. We find analytic expressions for the slow loss rate, with coefficients that depend on the particular decoherence mechanisms, thereby providing a means to probe, identify, and quantify various sources of decoherence with EIT. We go beyond the rotating wave approximation to consider how strong microwave fields can induce additional off-resonant transitions in the SQC, and we show how these effects can be mitigated by compensation of the resulting AC Stark shifts.

PACS numbers: 82.25.-j, 03.67.-a, 42.50.Gy

## I. INTRODUCTION

Superconducting quantum circuits (SQCs) based on Josephson junctions (JJs) exhibit macroscopic quantum-coherent phenomena [1]. These circuits exhibit quantized flux or charge states, depending on their fabrication parameters. The quantized states are analogous to the quantized internal (hyperfine and Zeeman) levels in an atom, and the SQCs thus behave like “artificial atoms.” Spectroscopy [2, 3, 4, 5], Rabi oscillations and Ramsey interferometry [6, 7, 8, 9, 10, 11, 12], cavity quantum electrodynamics [13, 14], and Stückelberg oscillations [15, 16] are examples of quantum-mechanical behavior first realized in atomic systems that have also been recently demonstrated with SQCs.

We recently leveraged the atom-SQC analogy to propose electromagnetically induced transparency (EIT) [17, 18] in superconducting circuits [19]. EIT has attracted much attention in atomic systems in the context of slow light [20], quantum memory [21, 22, 23] and nonlinear optics [24]. EIT occurs in so-called “ $\Lambda$ -systems” comprising two meta-stable states, each coupled via resonant electromagnetic fields to a third, excited state. For particular initial states called “dark states,” the absorption on *both* transitions is suppressed due to destructive quantum interference, thus making the atom transparent to the applied fields. Though EIT is often studied in the context of the behavior of a weak ‘probe’ field in the presence of a stronger ‘pump’ field, we focus on the case where the two fields have comparable amplitude. In Ref. [19], we analyzed a superconducting persistent-current qubit biased such that it exhibited a  $\Lambda$ -configuration: two meta-stable states (the qubit) and a third, shorter-lived state (the readout state). We showed that EIT provides a non-destructive means to confirm preparation of an arbitrary superposition state of the qubit. Moreover, we showed that the proposed EIT scheme can sensitively probe the qubit decoherence rate using a method analogous to the proposal in Ref. [25] for atomic systems. This method compliments other available techniques of probing decoherence such as spin echo [26] and Rabi oscillation decay [27]. Because the EIT method requires no manipulation of the qubit during the probing, it offers unique advantages in this regard. In addition to our EIT work, several groups have considered the use of “dark states” in SQCs comprising a  $\Lambda$ -configuration to implement adiabatic passage and its application to quantum information processing [28, 29, 30].

In the present work, we extend and augment our analysis in Ref. [19] with realistic effects which arise in SQCs due to the presence of additional quantized levels (beyond the three-level “ $\Lambda$ -system” model). These effects have qualitatively unique signatures in an EIT experiment, and

this work provides a tool for identifying their origin. This allows a more complete understanding of the full level-structure of the SQC system, and it further clarifies the necessary criteria for the experimental observation of EIT. The present work carries the spirit of previous investigations in which additional degrees of freedom (beyond two-level models) were required to explain quantitatively experimental Rabi oscillations in SQCs. Examples of these works include resonant tunneling across the barrier [31], diagonal dipole matrix elements [32], and coupling to additional degrees of freedom outside the SQC, such as micro-resonators [27, 33]. Just as EIT is sensitive to decoherence, it will be similarly sensitive to effects beyond the idealized three-level model.

The effects we investigate arise primarily from differences between SQCs and the atomic systems considered in much of the literature. First, while damping of the excited level is provided naturally by spontaneous emission in atoms, in SQCs, this decay is ‘manufactured’ by resonant biasing across the tunnel barrier followed by fast measurement with a SQUID. This process must be considered in more detail to assure this decay is indeed analogous to spontaneous decay in atoms. Second, the transitions are at microwave rather than optical frequencies, whereas the Rabi frequency coupling rates and dephasing rates tend to be faster than in atomic systems. This means that various couplings in the system can be more comparable to the level spacings and thus the rotating wave approximation (RWA) is often not as valid as in atomic systems. Third, the level structure itself is quite different. In particular, there is typically some degree of dipole-like coupling between *all* pairs of levels in the system, because selection rules allow all possible transitions [34]. Fourth, in SQCs, there is the possibility of direct resonant tunneling across the barrier, a feature which is absent in atomic systems.

This paper is organized in the following manner. In Section II, we introduce the proposed system, a persistent-current (PC) qubit [35, 36]. We discuss the conditions under which the PC qubit exhibits a  $\Lambda$ -configuration amongst its multi-level energy band structure that is conducive for an EIT demonstration. We then present the Hamiltonian and density matrix approaches to analyze the system dynamics. In Section III, we use the Hamiltonian approach to give useful analytic approximations to the full system, which allow us to investigate EIT in a reduced three-level system. We explore effects of population and phase mismatch between the prepared initial state and the desired dark state (as defined by the applied fields), and the effect of detuning the applied fields from their resonances. We also consider the SQUID measurement rate and its effect on the effective decay and frequency of the excited ‘read-out’ level. In Section IV, we use the density matrix approach to include pure dephasing and incoherent population loss and exchange,

generalizing our previous results in Ref. [19]. We explore the effect on EIT in the presence of coherent and incoherent tunneling processes. Generally, one must make the EIT ‘preparation rate’ (proportional to the microwave field intensities) faster than the decoherence rate in order to observe EIT. In Section V, we go beyond the rotating-wave approximation (RWA) to examine the important issue of microwave field-induced off-resonant transitions in the spirit of previous work on two-level systems [37]. We conclude that off-resonant transitions cause frequency shifts and losses which depend on the coupling field intensities. Unlike decoherence and detuning, these transitions generally manifest themselves as the field intensities are increased. The high-field frequency shifts are analogous to the AC-stark shifts observed in atomic systems. We show how the off-resonant effects can be mitigated and, in some cases, eliminated by compensating for the frequency shifts.

## II. THE PC-QUBIT

### A. The PC-qubit model

The persistent-current (PC) qubit is a superconductive loop interrupted by two Josephson junctions of equal size and a third junction scaled smaller in area by the factor  $0.5 < \alpha < 1$  (Fig. 1(a)) [35, 36]. Its dynamics are described by the Hamiltonian

$$\mathcal{H}_{pc} = \frac{1}{2}C \left( \frac{\Phi_0}{2\pi} \right)^2 (\dot{\varphi}_p^2 + (1 + 2\alpha)\dot{\varphi}_m^2) + E_j [2 + \alpha - 2 \cos \varphi_p \cos \varphi_m - \alpha \cos(2\pi f + 2\varphi_m)], \quad (1)$$

in which  $C$  is the capacitance of the larger junctions,  $\varphi_{p,m} \equiv (\varphi_1 \pm \varphi_2)/2$ ,  $\varphi_i$  is the gauge-invariant phase across the larger junctions  $i = \{1, 2\}$ ,  $E_j = I_c \Phi_0 / 2\pi$  is the Josephson coupling energy,  $I_c$  is the critical current of the larger junctions, and  $f$  is the magnetic flux through the loop in units of the flux quantum  $\Phi_0$  [36].

The qubit potential energy (the second term in  $\mathcal{H}_{pc}$ ) forms a 2D periodic double well potential, a one-dimensional slice through which is shown in Fig. 1(b). Each well corresponds to a distinct classical state of the electric current, *i.e.*, left or right circulation through the loop, with a net magnetization of that is discernable using a dc SQUID [36]. The relative depth of the two wells can be adjusted by detuning the flux bias to either side of the symmetric point  $f = 1/2$ . The potential wells exhibit quantized energy levels corresponding to the quantum states

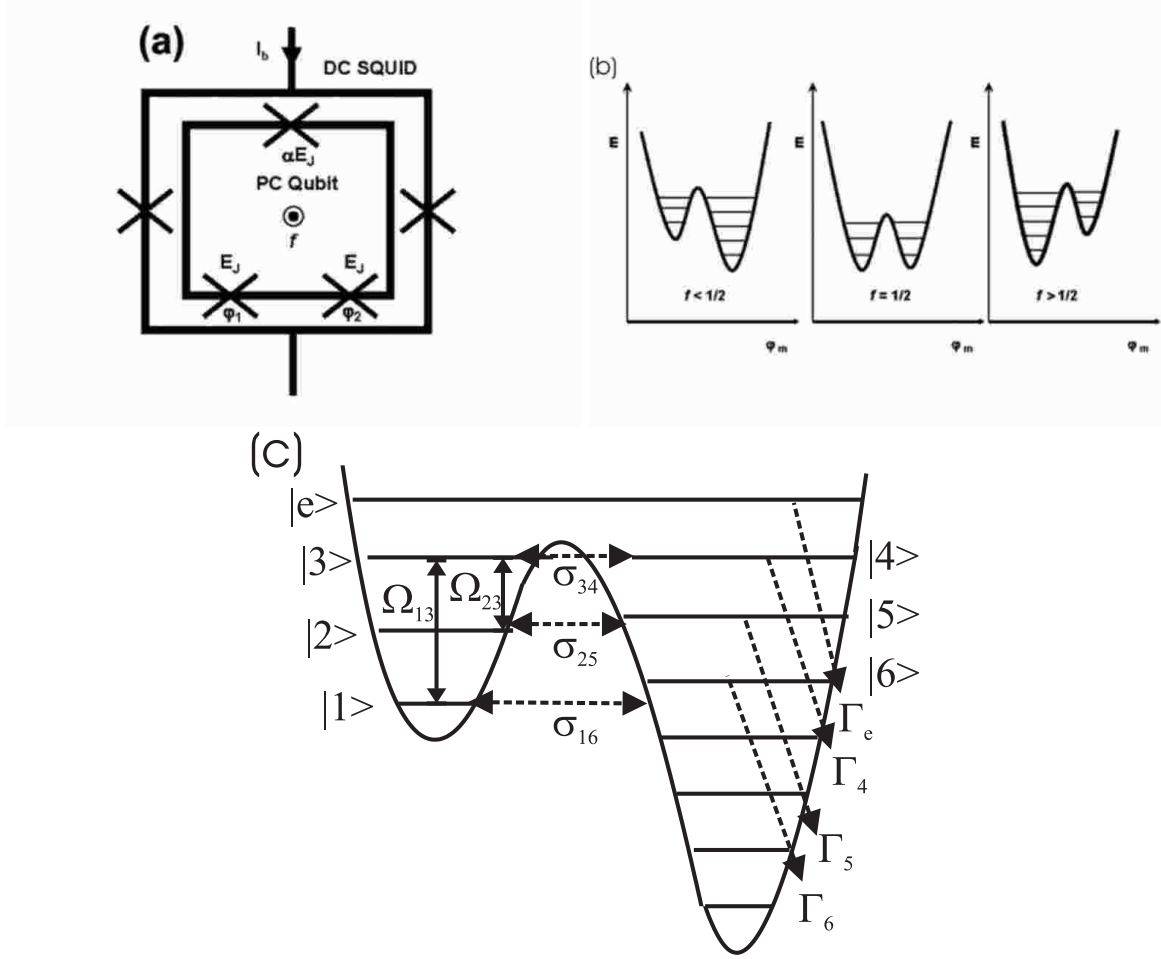


FIG. 1: **A pc-qubit with a dc SQUID measuring device** (a) A pc-qubit, a superconducting loop with two Josephson junctions of equal dimension and the third scaled by a factor  $\alpha$ , as shown in the inner loop. The outer loop is a dc-SQUID that is used to measure the magnetic moment of the qubit. (b) A representation of the potential energy of the pc-qubit as a function of  $f$ , the magnetic flux in the loop in units of the flux quantum  $\Phi_0$ . The qubit potential can range from an asymmetric double well biased to the right to a symmetric double well and to the an symmetric double well biased to the left for  $f$  ranging from  $< 1/2$ ,  $= 1/2$ , and  $> 1/2$  respectively. (c) One-dimensional double-well potential and energy-level diagram for  $f = 0.502$ , in which case we have a three-level system in the left-hand well. States  $|1\rangle$  and  $|2\rangle$  are meta-stable, while  $|3\rangle$  will have significant loss via resonant tunneling to  $|4\rangle$  ( $\sigma_{34}$ ). The right-hand well states undergo fast damping ( $\Gamma_4, \Gamma_5, \Gamma_6$ ) via the SQUID measurement and intrawell relaxation to lower states. Coupling between the our three-levels is induced by two resonant microwave fields with Rabi frequencies  $\Omega_{13}$  and  $\Omega_{23}$ , forming the  $\Lambda$ -system. The qubit parameters we use in calculations are  $\omega_2 - \omega_1 = (2\pi) 27.8$  GHz and  $\omega_3 - \omega_2 = (2\pi) 27$  GHz, with matrix elements  $x_{ij}$  for  $(i, j) = (1, 2), (2, 3)$ , and  $(1, 3)$  set to -0.0145, -0.0371, -0.0263, respectively.

of the macroscopic circulating current [38, 39, 40, 41], with the number of levels on each side determined by the depth and frequencies of the wells. In this basis the Hamiltonian can be written

$$\mathcal{H}_{pc} = \mathcal{H}_0 + \mathcal{H}_{\text{tunnel}}; \quad (2)$$

$$\mathcal{H}_0 = \hbar \sum_i \omega_i |i\rangle \langle i|, \quad (3)$$

$$\mathcal{H}_{\text{tunnel}} = \hbar \sum_{i,j \neq i} \sigma_{ij} |i\rangle \langle j|. \quad (4)$$

We note here that two points of view may be taken when discussing the system described by the Hamiltonian in Eq. (2). In one picture, the diabatic states (diagonal matrix elements) of the qubit are the uncoupled single-well states of classical circulating current, and these diabatic states are coupled through the tunneling terms (off-diagonal matrix elements). In a second picture, the Hamiltonian is diagonalized, resulting in eigenenergies and eigenstates of the double-well potential. Although the perspectives differ, these two pictures will, of course, lead to identical results; only the interpretation differs. Throughout the paper, we primarily describe the dynamics in terms of diabatic (single-well) states coupled through the tunneling barrier of the double-well potential and driven by harmonic excitation. Exceptions, where they exist, will be clearly noted.

The three-level  $\Lambda$  structure to implement EIT is then provided by the left-hand meta-stable states  $|1\rangle, |2\rangle$  and the fast decaying level  $|3\rangle$  shown in Fig. 1(c). Each of these levels are taken to have a finite loss rate  $\Gamma_i^{(t)}$ , due to resonant tunneling to a right-well state (at  $\sigma_{ij}$ ) followed by relaxation of the right-hand well state  $\Gamma_j$  (which is a sum of population relaxation to lower levels and damping induced by a fast SQUID measurement of the circulation current of right-hand well states). In particular, we desire a fast decay rate  $\Gamma_3^{(t)}$ , which is achieved by resonantly biasing  $|3\rangle$  and  $|4\rangle$  and a fast SQUID measurement ( $\approx 1$ -10 ns), as analyzed in Section III D. Conversely, we desire states  $|1\rangle$  and  $|2\rangle$  to be long-lived and the tunneling  $\sigma_{25}$  will cause loss and decoherence, which is analyzed in Section IV D ( $\sigma_{16}$  is negligible by comparison). Rough estimates of the interwell loss rates for *resonant*-tunneling are  $\Gamma_1^{(t)} \approx (1 \text{ ms})^{-1}$ ,  $\Gamma_2^{(t)} (1 \text{ } \mu\text{s})^{-1}$ , and  $\Gamma_3^{(t)} \approx (1 \text{ ns})^{-1}$  and the off-resonant biasing of states  $|1\rangle - |6\rangle$  and  $|2\rangle - |5\rangle$  will significantly decrease these rates. In addition, states  $|2\rangle$  and  $|3\rangle$  can have intrawell relaxation rates  $\Gamma_{3 \rightarrow 1}, \Gamma_{3 \rightarrow 2}, \Gamma_{2 \rightarrow 1}$  (not shown in the diagram). Under similar bias conditions the rate  $\Gamma_{3 \rightarrow 1} + \Gamma_{3 \rightarrow 2} \approx (25 \text{ } \mu\text{s})^{-1}$  (experimentally measured in [40]) is much slower than  $\Gamma_3^{(t)}$ . Also note that,  $\Gamma_{2 \rightarrow 1}$ , another source of decoherence of the meta-stable states, will be less than  $\Gamma_{3 \rightarrow 1} + \Gamma_{3 \rightarrow 2}$ .

These quantized levels may be coupled using microwave radiation. An applied radiation field  $\mu$  can be described in terms of an amplitude, frequency and phase:  $\Delta f_\mu = g_\mu \cos(\omega_\mu t + \phi_\mu)$ . We find the resulting matrix elements for level transitions (the Rabi frequencies) by treating  $\Delta f_\mu$  as a small perturbation in the  $\cos(2\pi f + 2\varphi_m)$  term in Eq. (1). We write it as  $\sin(2\pi f + 2\varphi_m) \sin(2\pi \Delta f_\mu)$ , which can be approximated as  $\sin(2\pi f + 2\varphi_m)(2\pi \Delta f_\mu)$ , leading to a Rabi frequency  $\Omega_{ij}^{(\mu)} \equiv (2\pi)g_\mu \alpha E_j x_{ij} / \hbar$ , where  $x_{ij} \equiv \langle i | \sin(2\pi f + 2\varphi_m) | j \rangle$ . The elements  $x_{ij}$  we calculate for our proposed parameters are listed in the caption of Fig. 1(c). In EIT, we address the SQC with two microwave fields  $\Delta f_a = g_a \cos(\omega_a t + \phi_a)$ , with  $\omega_a \approx \omega_3 - \omega_1$ , and  $\Delta f_b = g_b \cos(\omega_b t + \phi_b)$ , with  $\omega_b \approx \omega_3 - \omega_2$ . The microwave induced Hamiltonian can then be written as:

$$\mathcal{H}_{\mu\text{-wave}} = \frac{\hbar}{2} \sum_{i,j} \sum_{\mu} (\Omega_{ij}^{(\mu)} e^{-i(\omega_\mu t + \phi_\mu)} + c.c.) |i\rangle \langle j| \quad (5)$$

where  $i, j$  runs over the states and  $\mu$  runs over the two fields  $a, b$ . We emphasize that the above approximation is a perturbative approach valid only for small driving amplitudes. In the strongly driven limit, the approximation breaks down, preventing the Rabi frequency from growing without bound [7, 15].

Microwave excitation is used to establish the population of meta-stable states (such as  $|1\rangle$  and  $|2\rangle$ ) via *photon-assisted tunneling*. In this scheme, the population of a meta-stable state is driven via a resonant radiation field into a *read-out state* (i.e.  $|3\rangle$ ) which quickly tunnels to a *measurement state* (i.e.  $|4\rangle$ ). This state has opposing current circulation with a unique flux signature that can be measured using a DC-SQUID [36]. In the present scheme, *two* fields are simultaneously applied (resonant with  $|1\rangle \leftrightarrow |3\rangle$  and  $|2\rangle \leftrightarrow |3\rangle$ ; see Fig. 1(c)), and EIT is manifested by a suppression of the photon-assisted tunneling due to quantum interference between the two excitation processes.

## B. Evolution model

It is convenient to calculate dynamics from the above Hamiltonian terms in an interaction picture which transforms away the diagonal energies  $\mathcal{H}_0$  (3). In this frame the total Hamiltonian is then the sum of (4) and (5):

$$\tilde{\mathcal{H}} = \frac{\hbar}{2} \sum_{i,j} \sum_{\mu} (\Omega_{ij}^{(\mu)} e^{-i(\omega_\mu t + \phi_\mu)} + c.c.) e^{i(\omega_i - \omega_j)t} |i\rangle \langle j| + \hbar \sum_{i,j \neq i} \sigma_{ij} e^{i(\omega_i - \omega_j)t} |i\rangle \langle j| \quad (6)$$

Note that the exponential arguments involve sums of microwave frequencies  $\omega_\mu$  and level splittings  $\omega_i - \omega_j$ . When these nearly cancel the state is said to be near-resonant and the coupling is strong. However, for most of the terms, this cancellation does not occur, and the term rotates its phase rapidly on the scale of frequencies of interest ( $\Omega_{ij}^{(l)}$ ,  $\sigma_{ij}$  and  $\Gamma_j$ ). Such terms are neglected in the Rotating Wave Approximation (RWA).

We can also include incoherent losses from the levels,  $\Gamma_i$ , by introducing an additional non-Hermitian part of the Hamiltonian  $\tilde{\mathcal{H}}_{\text{relax}} = -i\hbar \sum_i (\Gamma_i/2) |i\rangle\langle i|$ . This is often done in quantum optics [42, 43] to include non-Hermitian decay of radiatively decaying levels. We then describe the system by a wavefunction  $|\tilde{\Psi}\rangle = \sum_i \tilde{c}_i(t) |i\rangle$ , with the initial population normalized to unity  $\sum_i |\tilde{c}_i(0)|^2 = 1$  (this can decay in time due to the non-Hermitian loss). The evolution of the  $|\tilde{\Psi}\rangle$  is governed from Schrödinger's equation:

$$i\hbar \frac{\partial}{\partial t} |\tilde{\Psi}\rangle = (\tilde{\mathcal{H}} + \tilde{\mathcal{H}}_{\text{relax}}) |\tilde{\Psi}\rangle. \quad (7)$$

Besides giving the coherent dynamics, this Schrödinger equation correctly predicts the population relaxation of level  $|i\rangle$  at  $\Gamma_i$  and also gives the correct dephasings of coherences between  $|i\rangle$  and other states at half this rate  $\Gamma_i/2$ .

When necessary, we use a density matrix approach to include incoherent processes. For example, pure dephasing of a coherence between the two meta-stable states  $|1\rangle$  and  $|2\rangle$  goes beyond the Hamiltonian approach (7). Similarly, incoherent feeding of levels (such as population into  $|1\rangle$  from interwell relaxation  $\Gamma_{2 \rightarrow 1}$ ) goes beyond this description. The density matrix is written  $\tilde{\rho} = \sum_{ij} \tilde{\rho}_{ij} |i\rangle\langle j|$ , where the population in the levels are given by the diagonal terms  $\tilde{\rho}_{ii}$  and correspond to  $|\tilde{c}_i|^2$  in the wavefunction description, while the off-diagonal terms  $\tilde{\rho}_{ij}$  correspond to  $\tilde{c}_i \tilde{c}_j^*$  and describe coherences between levels. The evolution of the density matrix is given by

$$i\hbar \frac{\partial}{\partial t} \tilde{\rho} = [\tilde{\mathcal{H}} + \tilde{\mathcal{H}}_{\text{relax}}, \tilde{\rho}] + \mathcal{L} \tilde{\rho}. \quad (8)$$

The first term reproduces the part already predicted by the Schrödinger equation (7), while the super-operator  $\mathcal{L}$ , the Lindbladian [42], accounts for other incoherent processes. For pure dephasing of the  $|i\rangle \leftrightarrow |j\rangle$  coherence,  $\gamma_{ij}$ , we introduce a term  $\mathcal{L}_{ij,ij} = -\gamma_{12}$ . For a population relaxation from  $|j\rangle \rightarrow |i\rangle$ ,  $\Gamma_{j \rightarrow i}$ , we introduce  $\mathcal{L}_{jj,ii} = +\Gamma_{j \rightarrow i}$ . The associated population loss from  $|j\rangle$  and decoherences are already included through Eq. 7 (via a term  $-i\hbar(\Gamma_{j \rightarrow i}/2) |i\rangle\langle i|$ ).

Throughout the paper, we consider the model in a number of distinct cases. In each, we include three levels  $|1\rangle, |2\rangle, |3\rangle$ , coupled by two microwave fields  $\Delta f_a, \Delta f_b$  making up our  $\Lambda$  system (see



Fig. 1(c)). We then selectively include additional levels, such as the  $|4\rangle$ ,  $|5\rangle$ , and  $|e\rangle$  to isolate the contributions of each of them. Numerical results were obtained with a fourth-order Runge-Kutta algorithm [44] solving Eq. (8). In it we do not make any RWA assumptions *a priori*, but instead introduce some cut-off frequency  $\omega_{RWA}$ . We examine the phase factors of each term in the evolution and set to zero ones with phases rotating faster than  $\omega_{RWA}$ .

We compare our numerical results with approximate analytic solutions in many cases. When possible, we use the Schrödinger equation (7) to obtain simpler analytic results, though the full density matrix approach is used when dephasing and interwell relaxation are considered (Sections IV A- IV C). In the analytic results we normally make an additional transformation  $|\tilde{\Psi}\rangle \rightarrow |\Psi\rangle$ ,  $\tilde{\mathcal{H}} + \tilde{\mathcal{H}}_{\text{relax}} \rightarrow \mathcal{H}$ , defined by transformations of each level frequency  $\{\tilde{c}_i\} \rightarrow \{c_i\} = \{\tilde{c}_i e^{i\delta_i t}\}$ , where the  $\delta_i$  are chosen in to eliminate time-dependent exponential phase factors in (6) (they are usually *detunings*, that is, frequency mismatches between the microwave frequencies and the corresponding transitions). Detuning from two-photon resonance, decoherence, and additional levels are all seen to destroy the perfect transparency of EIT and cause slow exponential loss of the population. We will obtain expressions for the loss rate  $R_L$  in these cases.

### III. ELECTROMAGNETICALLY INDUCED TRANSPARENCY IN A SQC

#### A. Ideal EIT in a $\Lambda$ configuration

We first consider the ‘ideal’ case in which the three levels in the left well (see Fig. 1(c)) are well isolated from direct tunneling to other levels, states  $|1\rangle$  and  $|2\rangle$  are perfectly stable, and  $|3\rangle$  quickly decays at some fast rate  $\Gamma_3^{(t)}$ . This decay is in reality due to resonant coupling of  $|4\rangle$  ( $\sigma_{34}$ ) and subsequent SQUID measurement  $\Gamma_4$ , but we will see in Section III D how one can derive  $\Gamma_3^{(t)}$  in terms of these underlying processes.

We apply fields with nearly resonant frequencies  $\omega_a = \omega_3 - \omega_1 + \Delta_{13}$  and  $\omega_b = \omega_3 - \omega_2 + \Delta_{23}$  (see Fig. 1(c)), where the  $\Delta_{13}, \Delta_{23}$  are small detunings. All other couplings are sufficiently detuned to safely eliminate them under the RWA. In this case the transformations to eliminate phase rotating terms are given by  $\delta_1 = 0$ ,  $\delta_2 = \Delta_{13} - \Delta_{23}$ ,  $\delta_3 = \Delta_{13}$ . The Hamiltonian, written in matrix notation in a basis  $\{|1\rangle, |2\rangle, |3\rangle\}$  is

$$\mathcal{H} = \frac{\hbar}{2} \begin{bmatrix} 0 & 0 & \Omega_{13}^* \\ 0 & -2\Delta_2 & \Omega_{23}^* \\ \Omega_{13} & \Omega_{23} & -i\Gamma_3^{(t)} - 2\Delta_{13} \end{bmatrix} \quad (9)$$

where  $\Delta_2 \equiv \Delta_{13} - \Delta_{23}$  is the detuning from *two-photon resonance*. Here we have dropped the  $a, b$  labels,  $\Omega_{13} \equiv \Omega_{13}^{(a)}$  and  $\Omega_{23} \equiv \Omega_{23}^{(b)}$  (see Eq. (6)) as there is no ambiguity. The open system loss of  $|3\rangle$  due to tunneling  $\Gamma_3^{(t)}$  is assumed to dominate incoherent population exchange due to intra-well relaxation, allowing a Schrödinger evolution analysis (7).

First consider the resonant case  $\Delta_{13} = \Delta_{23} = 0$ . A qubit initially in the ground state  $|1\rangle$  can be prepared in a superposition state  $|\Psi_{\text{init}}\rangle = c_1|1\rangle + c_2|2\rangle$  by temporarily driving it with a field resonant with the  $|1\rangle \leftrightarrow |2\rangle$  transition. Applying only one field  $\Omega_{13}$  ( $\Omega_{23}$ ) field then allows the population of a state  $|1\rangle$  ( $|2\rangle$ ) to be read out through a transition to state  $|3\rangle$  followed by a rapid escape to the right well. In this case, the superposition is destroyed by the absorption of a photon.

However, from (7) and (9) it follows that if we simultaneously apply both fields and the SQC is in the *dark* state

$$|\Psi_D\rangle = \frac{\Omega_{23}}{\Omega}|1\rangle - \frac{\Omega_{13}}{\Omega}|2\rangle, \quad (10)$$

(where  $\Omega \equiv \sqrt{|\Omega_{13}|^2 + |\Omega_{23}|^2}$ ) then (7) predicts  $\dot{c}_1 = \dot{c}_2 = \dot{c}_3 = 0$ . For this particular state, the two absorption processes,  $|1\rangle \leftrightarrow |2\rangle$  and  $|1\rangle \leftrightarrow |3\rangle$ , have equal and opposite probability amplitude and thus cancel by quantum interference. As a result, no excitation into  $|3\rangle$ , and thus no tunneling to the right well, will be observed. Note that  $|\Psi_D\rangle$  constrains both the relative intensity *and* phase of the light fields. Any other (non-zero) values for the relative amplitudes in the two states  $|1\rangle, |2\rangle$  will lead to a coupling into  $|3\rangle$  and subsequent loss.

An alternative interpretation is obtained by examining the eigensystem of the Hamiltonian (9). The dark state  $|\Psi_D\rangle$  has eigenvalue zero. The other two eigenstates are linear combinations of the excited state  $|3\rangle$  and the combination of the stable states orthogonal to  $|\Psi_D\rangle$ :  $|\Psi_A\rangle = (\Omega_{13}^*|1\rangle + \Omega_{23}^*|2\rangle)/\Omega$ , called the *absorbing state* (a “bright state”). The system  $\{|\Psi_A\rangle, |3\rangle\}$  acts effectively as a two-level system coupled by  $\Omega$ . The eigenvalues corresponding to the two eigenstates are  $(-i\Gamma_3^{(t)} \pm \sqrt{4\Omega^2 - \Gamma_3^{(t)2}})/4$  and the imaginary parts of these eigenvalues give the loss rates of these states. In the limit  $\Omega \gg \Gamma_3^{(t)}$ , these rates are both  $\Gamma_3^{(t)}/4$  and one observes damped Rabi oscillations. In the limit  $\Omega \ll \Gamma_3^{(t)}$ , there is an eigenstate  $\approx |\Psi_A\rangle$  with a slower damping rate

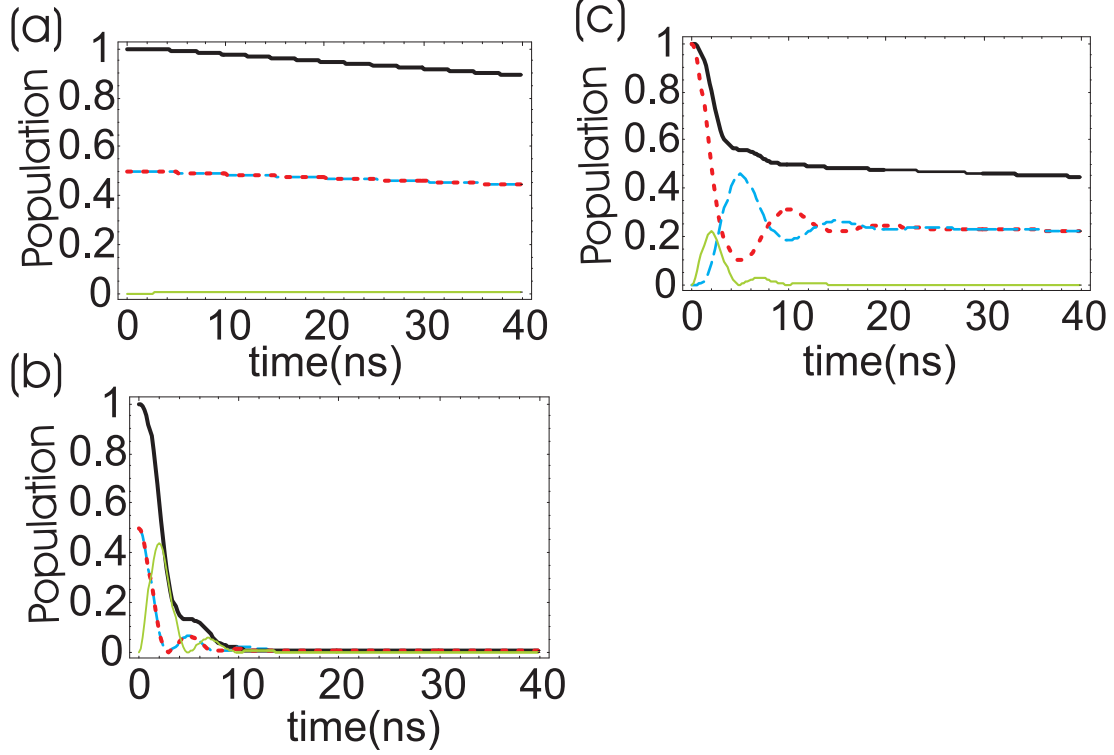


FIG. 2: (Color online) **Suppression of tunneling due to EIT for various ideal wavefunctions** (a) The populations of the states as a function of time in the presence of applied fields  $\Omega_{13} = \Omega_{23} = (2\pi) 150$  MHz and tunneling rate  $\Gamma_3^{(t)} = (2\pi) 130$  MHz =  $1/1.2$  ns for the initial state  $\rho_{11} = \rho_{22} = 0.5, \rho_{12} = -0.5$  (the dark state). The dotted (red) curve shows  $\rho_{11}$ , the dashed (blue)  $\rho_{22}$  and the thin solid (green)  $\rho_{33}$ . The total population (sum of the three) is the thick solid (black) curve. There is a slow exponential decay of the population due to the dephasing rate  $\gamma_{12} = (2\pi)1$  MHz. (b) The population evolutions (same convention) for the initial state  $\rho_{11} = \rho_{22} = 0.5, \rho_{12} = 0.5$  (the absorbing state). (c) The population evolutions for an initial state  $|1\rangle$  (which is an equal superposition of the dark and absorbing states).

$$\Omega^2/2\Gamma_3^{(t)}.$$

Figure 2(a) shows an example of the lack of tunneling in the presence of applied fields  $\Omega_{13} = \Omega_{23}$  for the corresponding dark state  $|\Psi_{\text{init}}\rangle = (|1\rangle - |2\rangle)/\sqrt{2}$  (i.e.  $\rho_{11} = \rho_{22} = 0.5, \rho_{12} = -0.5$ ). One sees only a barely perceptible population  $\rho_{33}$  and a very slow loss of the  $\rho_{11}$  and  $\rho_{22}$ . This is due to a pure dephasing of the state coherence, which we take to be  $\gamma_{12} = (2\pi) 1$  MHz. The effect of this dephasing is a small exponential loss at a rate we label  $R_L^{(\gamma_{12})}$ , which is discussed and derived in [19] and reviewed in Section IV B. Otherwise the populations remain  $\rho_{11} = \rho_{22} \approx 0.5$ . EIT thus provides a means to confirm, without disturbing the system, that one had indeed prepared

the qubit in a particular desired state of the SQC, preserving its quantum coherence.

By contrast, Fig. 2(b) shows the large loss induced when one applies these same fields to the absorbing state, *i.e.*, the state with the same populations but  $\pi$  out of phase:  $|\Psi_{\text{init}}\rangle = (|1\rangle + |2\rangle)/\sqrt{2}$ . In Fig. 2(b) we see that there is a large population in the  $|3\rangle$  and the entire population has tunneled to the right well within about 10 ns. Note that here we are in the intermediate regime  $\Omega \sim \Gamma_3^{(t)}$  so we get oscillations with period  $\sim \Omega$  strongly damped at  $\sim \Gamma_3^{(t)}/2$ . This is the completely analogous to the tunneling which occurs with a single applied field in a two-level scheme.

A general state can be decomposed into dark and absorbing state components. Fig. 2(c) shows a case where the initial population is purely in  $|1\rangle$  and the same fields are applied. Here the initial state can be written  $|\Psi_{\text{init}}\rangle = |1\rangle = (|\Psi_D\rangle + |\Psi_A\rangle)/\sqrt{2}$ . Half of the population (the component in the absorbing state) is coupled out over the 10 ns time scale while the dark state component remains. In terms of level populations  $\rho_{11}$ ,  $\rho_{22}$ , approximately 1/4 of the population is coherently coupled from  $|1\rangle$  to  $|2\rangle$ .

## B. EIT with imperfect state preparation

One of the useful aspects of EIT is the extremely sensitive manner in which it can measure the amplitude and phase of superpositions in the SQC. When the prepared state has a slightly different phase or population ratio than the state we intend to prepare, EIT could be used to measure these deviations. Such imperfect preparation could arise, for example, due to imperfections in the preparation pulse.

Fig.3(a), shows the populations loss when preparing a state with various initial state population ratios and applying fields  $\Omega_{13} = \Omega_{23}$ . We again introduce a small dephasing  $\gamma_{12} = (2\pi)1$  MHz. The inset shows the population at 200 ns, well after the initial transient losses have occurred. This data can be understood using the dark/absorbing basis discussed above. The modulus square of the overlap of the initial state and the dark state  $\langle\Psi_D|\Psi_{\text{init}}\rangle$  gives the population remaining after the fast initial loss of the absorbing component. Postulating that the slower loss (due to dephasing or other effects) is exponential with some rate  $R_L$ , the population after the fast initial loss is:

$$|\langle\Psi_{\text{init}}|\Psi_D\rangle|^2 e^{-R_L t}. \quad (11)$$

Thus, detecting the fast initial decay of the population can indicate the mismatch between the fields

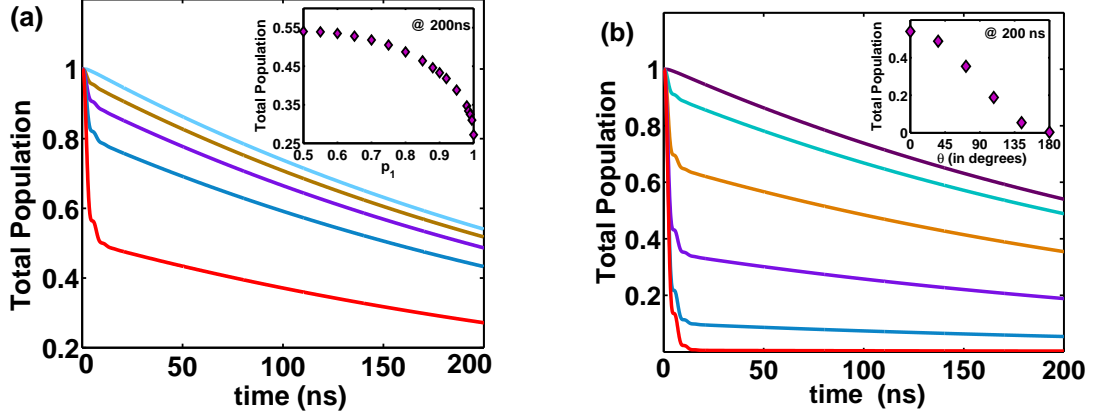


FIG. 3: (Color online) **Imperfect state preparation**(a) The time evolution of the population in the left well as a function of initial state of the form  $|\Psi_{\text{init}}\rangle = \sqrt{p_1}|1\rangle - \sqrt{(1-p_1)}|2\rangle$ . The uppermost curve is for the dark state  $p_1 = 0.5$ . Successively lower curves are for  $p_1 = 0.6, 0.7, 0.8, 0.9$  and  $1.0$ . There is a sharp initial decay when there are deviations from the dark state. Inset: The population in the left well at 200 ns versus  $p_1$ . (b) The population decay out of the left well as a function of the initial phase of the prepared state,  $|\Psi_{\text{init}}\rangle = (|1\rangle - e^{i\theta}|2\rangle)/\sqrt{2}$ .  $\theta = 0$  (top curve) and the other curves are  $\pi/5, 2\pi/5, 3\pi/5, 4\pi/5$ , and  $\pi$ . We see full decay for  $\theta = \pi$ , the absorbing state  $|\Psi_A\rangle = (|1\rangle + |2\rangle)/\sqrt{2}$ . Inset: The population in the left well at 200 ns as a function of  $\theta$ .

and the prepared state population.

Phase mismatch, or unwanted  $z$ -rotation, in the qubit preparation shows similar behavior. Figure 3(b) shows the population decay from the left well for the state  $(|1\rangle - e^{i\theta}|2\rangle)/\sqrt{2}$ . The uppermost line is decay due to the perfect state, while the lower lines indicate the decay for varying value of  $\theta$ . This example indicates that the dark state, is more sensitive to phase mismatch than population mismatch.

### C. EIT detuned from resonance

Because EIT is a coherent effect, it only occurs in a narrow range of frequencies near the two-photon resonance. The width of the EIT feature is generally determined by the field intensities, and can be made narrower than the broad resonances of the individual one-photon transitions ( $|1\rangle \leftrightarrow |3\rangle$  and  $|2\rangle \leftrightarrow |3\rangle$ ), which are determined by the fast decay rate of  $|3\rangle$   $\Gamma_3^{(t)}$ .

Figure 4(a) shows the results of simulations with the same parameters as Fig. 2(a), but with the

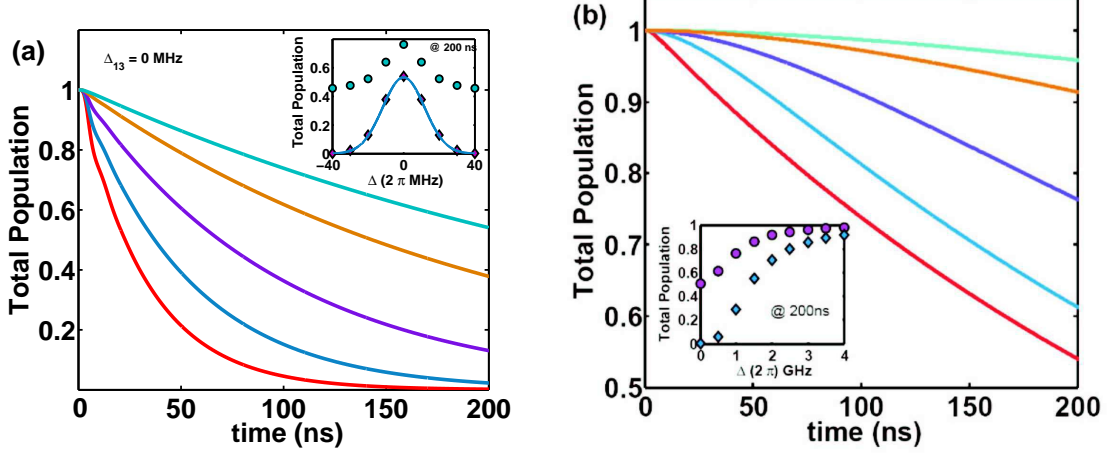


FIG. 4: (Color online) **EIT in the presence of detuning.** (a) Numerical calculation of the total population in time when  $\Delta_{13} = 0$  MHz, and at various  $\Delta_{23}$  (top to bottom curve)  $(2\pi)$  0, 10, 20, 30, 40 MHz. For  $\Delta_{23} = 0$ , the decay is due to pure dephasing, while the decay is sharper when  $\Delta_{23} \neq 0$ . Inset: The population in the left well at 200 ns as a function of the two-photon detuning  $\Delta_2 \equiv \Delta_{13} - \Delta_{23}$ , with  $\Delta_{13} = 0$  (circles). The solid curve shows the prediction (13). The diamonds show the case  $\Delta_{13} = (2\pi)1$  GHz, varying  $\Delta_2$  about the two-photon resonance. (b) The population decay as a function one-photon detuning at two-photon resonance,  $\Delta_{13} = \Delta_{23} = \Delta$  for (top to bottom)  $(2\pi)$  3, 2, 1, 0.5, 0 GHz. As the one-photon detuning increases, the effective coupling of the fields to the transition reduces, hence reducing the rate of decay. Inset: The population in the left well at 200 ns as a function of the detuning for the dark state (circles). For comparison we also show the population remaining for the absorbing state  $|\Psi_{\text{init}}\rangle = (|1\rangle + |2\rangle)/\sqrt{2}$  at the same detunings (diamonds).

detuning  $\Delta_{23}$  varied. The curves show exponential loss occurring at various rates. We can analyze the results with the Hamiltonian (9) and the corresponding Schrödinger equation (7). We first adiabatically eliminate [45] the excited level by setting  $\dot{c}_3 = 0$  and obtain

$$c_3 = (\Omega_{13}c_1 + \Omega_{23}c_2) \left( \frac{2\Delta_{13} - i\Gamma_3^{(t)}}{4\Delta_{13}^2 + \Gamma_3^{(t)2}} \right) \quad (12)$$

This expression is valid for times long compared to the initial transient time  $\text{Min}\{(\Gamma_3^{(t)})^{-1}, \Delta_{13}^{-1}\}$ . Note that for the dark state (10) the amplitude  $c_3$  vanishes. Plugging this expression back into the equations for  $\dot{c}_1, \dot{c}_2$  then gives a  $2 \times 2$  matrix evolution equation, which can be easily solved by finding for its eigenvalues and eigenvectors. For  $\Delta_2 = 0$  the eigenvectors are simply the dark  $|\Psi_D\rangle$  and absorbing  $|\Psi_A\rangle$  states of Section III A, with eigenvalues  $\lambda_D = 0$  and  $\lambda_A = -\Omega^2(\Gamma_3^{(t)} -$

$2i\Delta_{13})/2(4\Delta_{13}^2 + \Gamma_3^{(t)^2})$ , respectively. The absorbing component population is damped out at  $-2\text{Re}\{\lambda_A\}$ . In many cases, we are interested in the regime close to the one-photon resonance  $\Delta_{13} \ll \Gamma_3^{(t)}$  for which this reduces to  $\Omega^2/\Gamma_3^{(t)}$  as in Section III A.

With a non-zero two-photon detuning  $\Delta_2$ , this process is complicated an additional phase evolution term. Plugging (9) into Schrödinger's equation (7) (in the frame defined before (9)) gives a term  $\dot{c}_2 = \dots + i\Delta_2 c_2$ , which acts to drive the phase of the SQC out of the dark state and competes with damping of the absorbing component. Solving for the eigensystem in this case we see that, in the limit of small two-photon detuning ( $|\Delta_2| \ll |\text{Re}\{\lambda_A\}|$ ), the eigenvalue corresponding to the dark component has a non-zero negative real component, leading to a population loss rate:

$$-2\text{Re}\{\lambda_D\} \equiv R_L^{(\Delta_2)} = 4 \frac{|\Omega_{13}|^2 |\Omega_{23}|^2}{\Omega^4} \frac{\Delta_2^2 \Gamma_3^{(t)}}{\Omega^2} \quad (13)$$

The prediction  $P = \exp[-(R_L^{(\gamma_{12})} + R_L^{(\Delta_2)})t]$  is plotted in the inset of Fig. 4(a) and is seen to agree well with the numerical results (where  $R_L^{(\gamma_{12})}$  was determined by the numerically calculated loss for  $\Delta_{23} = 0$ ). Eq. (13) shows how the field strength, via  $\Omega^2$  in the denominator, determines the frequency width of the EIT feature.

The above analysis indicates that it is only the two-photon detuning  $\Delta_2$  which effects the relative phase of  $|1\rangle$  and  $|2\rangle$  and therefore effects the dark state. EIT will occur in the presence of a large one-photon detuning  $\Delta_{13}$  and the inset of Figure 4(a) shows such a case with  $\Delta_{13} = (2\pi) 1$  GHz and  $\Delta_{23}$  varied about the two-photon resonance. The presence of a transparency peak is still clear. The important difference is, because of the large one-photon detuning  $\Delta_{13} \gg \Gamma_3^{(t)}$ , the damping of the absorbing state  $-2\text{Re}\{\lambda_A\}$  is substantially reduced and so both the dephasing  $R_L^{(\gamma_{12})}$  and detuning  $R_L^{(\Delta_2)}$  loss are reduced. The analytic model (13) is not valid for large one-photon detunings  $\Delta_{13}$  where the strong damping assumption  $-2\text{Re}\{\lambda_A\} \gg |\Delta_2|$  does not hold. As a result, one sees non-exponential decay in the large one-photon detuning cases (upper curves of Fig. 4(b)).

Figure 4(b) shows simulations at two-photon resonance  $\Delta_{13} = \Delta_{23}$ , varying the one-photon detuning  $\Delta_{13}$ . The population decay is much slower as the detuning gets larger. For comparison, we also plot the decay for initial state equal to the absorbing state  $|\Psi_{\text{init}}\rangle = (|1\rangle + |2\rangle)/\sqrt{2}$ . We note that the analytic model for loss of the dark state (13) is invalid for large one-photon detunings, where the absorbing state is not completely damped.

#### D. Effective $\Lambda$ -system via tunneling and measurement

Thus far we have considered the system to be a three level system with the excited level  $|3\rangle$  subject to a fast population decay  $\Gamma_3^{(t)}$ . Underlying this decay are actually two processes: the fast resonant tunneling to a near degenerate level in the right hand well ( $\sigma_{34}$ ) followed by interwell relaxation and possibly a strong measurement of the population in  $|4\rangle$  ( $\Gamma_4$ ); see Fig. 1(c). We show here how the picture of a three-level system with a strong damping of  $|3\rangle$  (the Hamiltonian (9)) is most valid when  $\sigma_{34} < \Gamma_4$  but actually has a larger range of validity than one might expect. We derive an expression for  $\Gamma_3^{(t)}$  and also see how the tunneling slightly shifts  $\omega_3$ .

To do this we consider the Schrödinger evolution of the full four-level system Hamiltonian (with the same frame transformation as Eq. (9) and  $\delta_4 = \Delta_{13} + \delta_{34}$ , where  $\delta_{34} = \omega_4 - \omega_3$ ):

$$\mathcal{H} = \frac{\hbar}{2} \begin{bmatrix} 0 & 0 & \Omega_{13}^* & 0 \\ 0 & -2\Delta_2 & \Omega_{23}^* & 0 \\ \Omega_{13} & \Omega_{23} & -2\Delta_{13}^{(0)} & 2\sigma_{34} \\ 0 & 0 & 2\sigma_{34} & -i\Gamma_4 - 2(\Delta_{13}^{(0)} + \delta_{34}) \end{bmatrix}, \quad (14)$$

We have used the notation  $\Delta_{13}^{(0)}$  to distinguish it from  $\Delta_{13}$  which includes the frequency shift of  $\omega_3$  induced by  $|4\rangle$ .

To recover our three-level picture, we note that when  $\Gamma_4 \gg \sigma_{34}$  we can adiabatically eliminate level  $|4\rangle$  to obtain  $c_4 = -2c_3\sigma_{34}/[2(\delta_{34} + \Delta_{13}^{(0)}) - i\Gamma_4]$ . Plugging this result back into the equation for  $\dot{c}_3$  reveals that our system can be reduced to a three-level system as in (9) with  $\Gamma_3^{(t)} = 4|\sigma_{34}|^2\Gamma_4/[\Gamma_4^2 + 4(\delta_{34} + \Delta_{13}^{(0)})^2]$  and  $\Delta_{13} = \Delta_{13}^{(0)} + 4|\sigma_{34}|^2\delta_{34}/[\Gamma_4^2 + 4(\delta_{34} + \Delta_{13}^{(0)})^2]$ . Alternatively, when  $\Gamma_4 \ll \sigma_{34}$  we would expect the tunneling to induce a splitting of  $|3\rangle$  and  $|4\rangle$  into two superposition eigenstates (split by  $2\sigma_{34}$ ).

We carried out several numerical simulations of the four-level density matrix equations (8) for this system, considering first the resonant case ( $\delta_{34} = 0$ ). In them we used  $\sigma_{34} = (2\pi)150$  MHz =  $(1.2 \text{ ns})^{-1}$ , fields  $\Omega_{13} = (2\pi)120$  MHz,  $\Omega_{23} = (2\pi)150$  MHz, the corresponding dark initial state  $\rho_{11} = 0.61, \rho_{22} = 0.39, \rho_{12} = -\sqrt{\rho_{11}\rho_{22}}$  (*i.e.* full coherence), and a dephasing rate  $\gamma_{12} = (2\pi)2$  MHz. Figure 5(a) shows the populations  $\rho_{33}, \rho_{44}$  versus time for cases  $\Gamma_4^{-1} = 1 \text{ ns} = ((2\pi)159 \text{ MHz})^{-1}$  (thin, blue curves) and  $25 \text{ ns} = ((2\pi)6 \text{ MHz})^{-1}$  (thick, red curves). Fig. 5(b) shows the total population remaining versus time. In the fast measurement case, 1 ns,  $\rho_{33}$  and  $\rho_{44}$  are seen to track each other, and we see the exponential decay of the population as in the



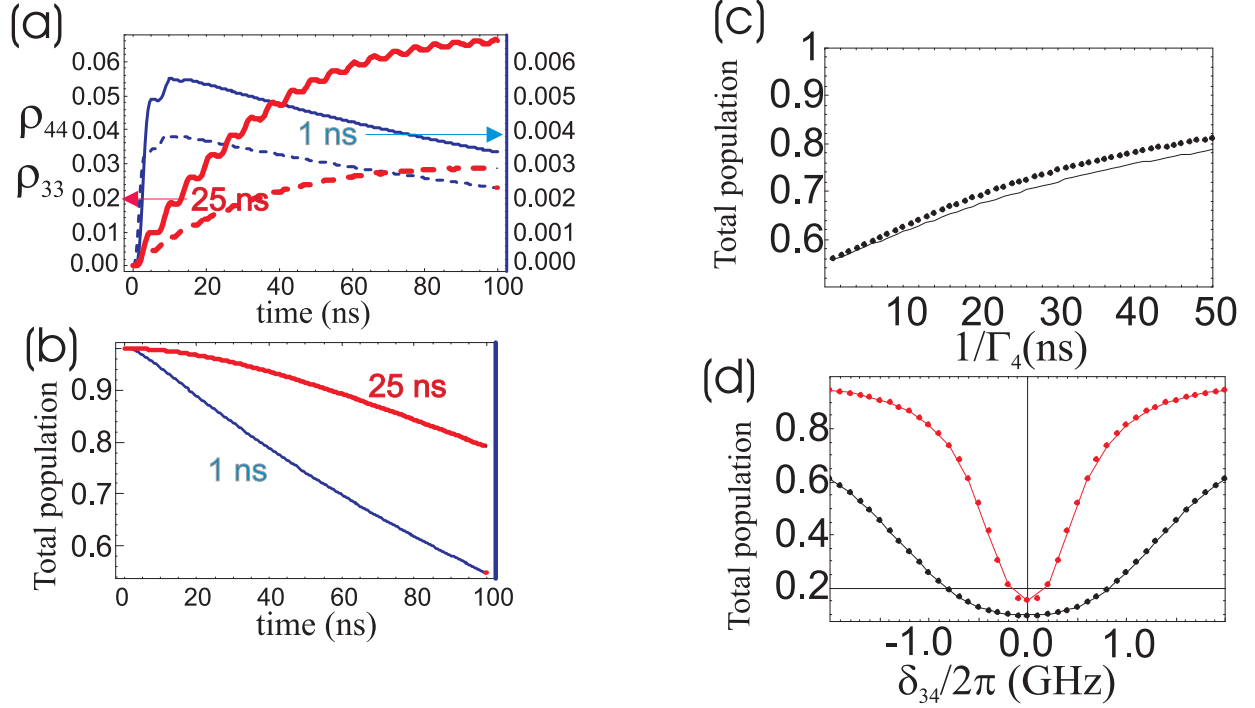


FIG. 5: (Color online) **Consequences of the measurement state characteristics.** (a) The thinner curves (blue) show populations  $\rho_{44}$  (solid curves) and  $\rho_{33}$  (dashed) as a function of time for a fast read-out  $\Gamma_4^{-1} = 1 \text{ ns} < \sigma_{34}^{-1}$  (with scale on the right side). After initial transient period, the two values reach quasi-steady state values, which undergo slow exponential decay. Conversely the thick (red online) curves show a slow measurement case  $\Gamma_4^{-1} = 25 \text{ ns} \gg \sigma_{34}^{-1}$  (scale on the left). In this case the populations do not reach a quasi-steady over the time scale plotted. (b) The total population remaining versus time for the same two cases. (c) The population remaining at 100 ns for varying measurement rates (dots) and compared to the prediction of a three-level system with  $\Gamma_3^{(t)}$ . As the measurement gets slower, this prediction slightly and increasingly underestimates the actual population which should be observed. (d) Numerical results (dots) and three-level model predictions (solid curves) now letting  $\delta_{34}$  vary, for the cases  $\Gamma_4^{-1} = 1 \text{ ns}$  (black, lower curve) and 10 ns (upper, red curve).

previous examples. For the slower measurement case, 25 ns, we see  $\rho_{33}$  and  $\rho_{44}$  still track each other, but here there is a large excitation  $\rho_{33}$  (note the different scale), no fast transients in  $\rho_{33}$  to a quasi-steady state value, and non-exponential population decay, all indications of the breakdown of EIT.

To check the validity of the effective three-level model, in Fig. 5(c) we compare its predictions for the populations remaining after 100 ns (solid curve) with predictions of the full four-level

model (dots). The agreement is excellent for the  $1/\Gamma_4 \leq 5$  ns, and is still in rough agreement even up to 50 ns. The adiabatic elimination procedure appears to be valid well beyond the expected regime  $\Gamma_4^{-1} \ll \sigma_{34}^{-1}$ . The breakdown of EIT in the 25 ns case is due to  $\Gamma_3^{(t)}$  becoming too large (see Section IV B), rather than a breakdown of the effective three-level model.

In Fig. 5(d) we show the population remaining for when  $\delta_{34}$  is varied (for both  $1/\Gamma_4 = 1$  ns (black curves) and 10 ns (red curves)). We have kept the microwave fields on bare resonance  $\Delta_{13}^{(0)} = \Delta_{23}^{(0)} = 0$  and accounted for the predicted frequency shifts of  $\omega_3$  in the three-level model. As  $\delta_{34}$  becomes comparable to  $\Gamma_4$  the tunneling rate  $\Gamma_3^{(t)}$  goes down as predicted.

In summary, we find that so long as  $\Gamma_4 > \sigma_{34}$  the simple three-level provides an excellent model and even when  $\Gamma_4 \sim \sigma_{34}$  or somewhat larger, this model unexpectedly gives very good predictions of the behavior. However, one must be careful of the strong dependence of  $\Gamma_3^{(t)}$  on  $\Gamma_4$ , as this may severely effect the necessary conditions for EIT (which are discussed in Section IV B). Through  $\Gamma_4$  the SQUID measurement rate can thus have a large influence on the EIT. When the detuning  $\delta_{34}$  becomes comparable to  $\Gamma_4$  the tunneling rate is reduced as expected and one must account for the frequency shift of  $\omega_3$ . For the remainder of the paper, we will not explicitly include  $|4\rangle$  in the calculations, but assume some  $\Gamma_3^{(t)} \sim 1$  ns and that the frequency shift is already included in the definitions of  $\Delta_{13}, \Delta_{23}$ .

#### IV. EIT IN THE PRESENCE OF DECOHERENCE, INCOHERENT POPULATION EXCHANGE, AND QUBIT TUNNELING

An outstanding, important issue in the eventual application of SQCs to quantum computing is the identification and suppression of sources of decoherence and unwanted dynamics of the qubit states ( $|1\rangle$  and  $|2\rangle$ ). In particular, decoherence from pure dephasing [46], intrawell relaxation, interwell resonant tunneling [31], and coupling to microscopic degrees of freedom in the junction [27] have all been proposed as potential hurdles in successfully isolating a coherent two-level system for use as a qubit. Use of phase sensitive methods such as EIT could be a fruitful path for exploring and differentiating the contributions of these various decoherence processes to qubit dynamics. To learn how EIT is effected by decoherence, we use the density matrix approach here to include pure dephasing, population loss, incoherent population exchange, and resonant coupling to the right well. We find a minimum microwave coupling strength necessary for the observation of EIT in the presence of decoherence and see it contributes small exponential loss (as seen in the

numerical results above). We derive analytic expressions for the loss rates, which are proportional to the decoherence processes but with coefficients which depend on the nature of the process. These results are a generalization of the results for pure dephasing previously published [19].

EIT is a unique tool to probe decoherence which compliments the previously explored techniques of spin echo [26] and Rabi oscillation decay [27], and this section will demonstrate some of its advantages. First, in the limit of small decoherence, the system is left completely undisturbed by the probe. Second, the dependence of the loss rates on relative field strengths can be used to determine the nature of the decoherence process. Third, the populations of the qubit states  $|1\rangle$   $|2\rangle$  do not need to be manipulated in the process (with  $\pi$  pulses, etc.). Besides the advantage of simplicity, this latter point also leaves open the possibility of decoherence rates which have a non-trivial dependence on the relative state populations.

### A. Density matrix approach

To carry out this analysis, we must go beyond the Schrödinger approach, and introduce the corresponding density matrix evolution (8), also referred to as the Bloch equations [42]. We work in the three-level case and transform to the frame defined above Eq. (9) and obtain:

$$\begin{aligned}
\dot{\rho}_{11} &= -\Gamma_1^{(t)} \rho_{11} + \Gamma_{2 \rightarrow 1} \rho_{22} - \frac{i}{2} \Omega_{13}^* \rho_{31} + \frac{i}{2} \Omega_{13} \rho_{13}, \\
\dot{\rho}_{22} &= -(\Gamma_2^{(t)} + \Gamma_{2 \rightarrow 1}) \rho_{22} - \frac{i}{2} \Omega_{23}^* \rho_{32} + \frac{i}{2} \Omega_{23} \rho_{23}, \\
\dot{\rho}_{33} &= -\Gamma_3^{(t)} \rho_{33} + \frac{i}{2} \Omega_{13}^* \rho_{31} - \frac{i}{2} \Omega_{13} \rho_{13} + \frac{i}{2} \Omega_{23}^* \rho_{32} - \frac{i}{2} \Omega_{23} \rho_{23}, \\
\dot{\rho}_{12} &= -\left(\gamma_{12} + \frac{\Gamma_1^{(t)} + \Gamma_2^{(t)} + \Gamma_{2 \rightarrow 1}}{2}\right) \rho_{12} - \frac{i}{2} \Omega_{13}^* \rho_{32} + \frac{i}{2} \Omega_{23} \rho_{13}, \\
\dot{\rho}_{13} &= -\frac{\Gamma_3^{(t)} + \Gamma_1^{(t)}}{2} \rho_{13} + \frac{i}{2} \Omega_{13}^* (\rho_{11} - \rho_{33}) + \frac{i}{2} \Omega_{23}^* \rho_{12}, \\
\dot{\rho}_{23} &= -\frac{\Gamma_3^{(t)} + \Gamma_2^{(t)} + \Gamma_{2 \rightarrow 1}}{2} \rho_{23} + \frac{i}{2} \Omega_{23}^* (\rho_{22} - \rho_{33}) + \frac{i}{2} \Omega_{13}^* \rho_{21}.
\end{aligned} \tag{15}$$

For simplicity, we have supposed the resonant case  $\Delta_{13} = \Delta_{23} = 0$  and ignored inter-well relaxation of  $|3\rangle$ , which is dominated by  $\Gamma_3^{(t)}$ . The remaining three elements equations are determined by  $\rho_{ij}^* = \rho_{ji}$ . The most important new piece here is the decoherence rate of  $\rho_{12}$ :  $\gamma_{12} + (\Gamma_1^{(t)} + \Gamma_2^{(t)} + \Gamma_{2 \rightarrow 1})/2$ . This will decohere the dark state and lead to the small losses in the population.

To proceed, we adiabatically eliminate the excited state coherences  $\rho_{13}, \rho_{23}$  as they are strongly damped by  $\Gamma_3^{(t)}$ . In these equations we can ignore  $\Gamma_1^{(t)}, \Gamma_2^{(t)} \ll \Gamma_3^{(t)}$  as well as  $\rho_{33} \ll \rho_{11}, \rho_{22}$ . We then plug the results back into the remaining equations to obtain:

$$\begin{aligned}\dot{\rho}_{11} &= -\Gamma_1^{(t)}\rho_{11} + \Gamma_{2 \rightarrow 1}\rho_{22} - \frac{|\Omega_{13}|^2}{\Gamma_3}\rho_{11} - \left(\frac{\Omega_{13}\Omega_{23}^*}{2\Gamma_3}\rho_{12} + \text{c.c.}\right), \\ \dot{\rho}_{22} &= -(\Gamma_2^{(t)} + \Gamma_{2 \rightarrow 1})\rho_{22} - \frac{|\Omega_{23}|^2}{\Gamma_3}\rho_{22} - \left(\frac{\Omega_{13}\Omega_{23}^*}{2\Gamma_3}\rho_{12} + \text{c.c.}\right), \\ \dot{\rho}_{12} &= -\left(\gamma_{12} + \frac{\Gamma_1^{(t)} + \Gamma_2^{(t)} + \Gamma_{2 \rightarrow 1}}{2}\right)\rho_{12} - \frac{\Omega^2}{2\Gamma_3^{(t)}}\rho_{12} - \frac{\Omega_{13}^*\Omega_{23}}{2\Gamma_3^{(t)}}(\rho_{11} + \rho_{22})\end{aligned}\quad (16)$$

We note here a strong damping of the coherence provided by the fields  $\Omega^2/2\Gamma_3^{(t)}$ . This damping acts to drive the system into the dark state. In the limit that the decoherence terms ( $\gamma_{12}, \Gamma_1^{(t)}, \Gamma_2^{(t)}, \Gamma_{2 \rightarrow 1}$ ) vanish, there is a steady state solution consisting of perfect coherence:  $\rho_{11} = |\Omega_{23}|^2/\Omega^2$ ,  $\rho_{22} = |\Omega_{13}|^2/\Omega^2$ ,  $\rho_{12} = -\Omega_{13}\Omega_{23}/\Omega^2$ . However, the decoherence terms drive the system out of the dark state, causing excitation  $\rho_{33}$ . One sees the ratio of the decoherence rate compared with the EIT preparation rate  $\Omega^2/\Gamma_3^{(t)}$  determines the degree to which the coherence deviates from the perfect dark state value.

## B. Measuring dephasing with EIT

We first show this comes into play for the pure dephasing, which is expected to be the case in many practical implementations and was analyzed previously in [19]. Figure 6(a) (solid, red curve) shows the excited state population  $\rho_{33}$  when  $\gamma_{12} = (2\pi)1$  MHz and we apply the fields  $\Omega_{13} = \Omega_{23} = (2\pi)150$  MHz to the dark state  $|\Psi_{\text{init}}\rangle = |\Psi_D\rangle = (|1\rangle - |2\rangle)/\sqrt{2}$ . One sees a small (note the scale in Fig. 6(a)) but finite excitation. In particular, there is an initial fast transient behavior to some plateau value (over a time scale determined by  $\text{Min}\{\Omega^2/\Gamma_3^{(t)}, \Gamma_3^{(t)}\}$ ), followed by a slow exponential decay. The general behavior of an initial transient rise, Fig. 6(a), was seen over a wide parameter regime. This quasi-steady state excitation of  $|3\rangle$  is the origin of the exponential losses at rate  $R_L^{(\gamma_{12})}$  in the previous simulations. Fig. 6(b) shows the exponential decay for several different dephasing rates  $\gamma_{12}$ . The inset of Fig. 6(b) plots the populations remaining at 200 ns, which is seen to approach unity as  $\gamma_{12} \rightarrow 0$ .

The loss rate can be quantified by considering the  $3 \times 3$  evolution matrix for  $\rho_{11}, \rho_{22}$ , and  $\rho_{12}$  defined by (16). Looking at the eigenvalue corresponding to the smallest loss rate, and expanding

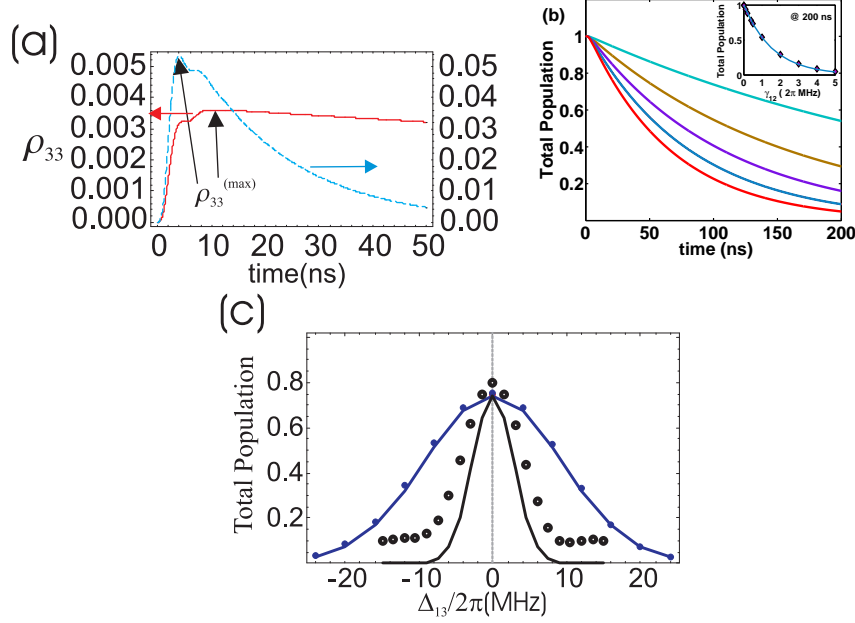


FIG. 6: (Color online) **EIT loss due to pure dephasing** (a) The population  $\rho_{33}$  versus time in the presence of a pure dephasing  $\gamma_{12} = (2\pi)1$  MHz (solid, red curve, scale on left) and  $\gamma_{12} = (2\pi)20$  MHz (dashed, blue curve, scale on right). In the slow dephasing case  $\rho_{33}$  quickly reaches a plateau value  $\rho_{33}^{(\max)}$  then undergoes a slow exponential decay. For the faster dephasing, the exponential decay time is similar to the time required to reach the maximum value. In each case, the initial state is  $\rho_{11} = \rho_{22} = 0.5$  and  $\rho_{12} = -0.5$ ,  $\Omega_{13} = \Omega_{23} = (2\pi)150$  MHz and  $\Gamma_3^{(t)} = (2\pi)130$  MHz (b) The population decay with varying dephasing rates (top curve to bottom curve)  $\gamma_{12} = (2\pi) 1, 2, 3, 4$ , and  $5$  MHz. Inset: The population in the left well at  $200$  ns versus  $\gamma_{12}$  (dots). The solid curve shows the analytic prediction  $\exp(-R_L^{(\gamma_{12})}t)$  based on Eq. 17, demonstrating how the population loss can be used as a probe of  $\gamma_{12}$ . (c) Population remaining at  $100$  ns versus detuning  $\Delta_{13}$  (keeping  $\Delta_{23} = 0$ ) for two different field intensities. In these simulations we used the initial conditions  $\rho_{11} = 0.61$ ,  $\rho_{22} = 0.39$ ,  $\rho_{12} = -\sqrt{\rho_{11}\rho_{22}}$ , the fields  $\Omega_{13} = 0.8\Omega_{23}$ ,  $\Gamma_3^{(t)} = (2\pi)159$  MHz,  $\gamma_{12} = (2\pi)1$  MHz. The solid curves are the analytic prediction described in the text for  $\Omega_{23} = (2\pi)100$  MHz (blue, upper curve), and  $30$  MHz (black, lower curve). The dots show the numerical results.

to first order in  $\gamma_{12}$  gives:

$$R_L^{(\gamma_{12})} = 2\gamma_{12} \frac{|\Omega_{13}|^2 |\Omega_{23}|^2}{\Omega^4} \quad (17)$$

By measuring this decay constant experimentally, one can use (17) to extract  $\gamma_{12}$ . Note that the

two rates are simply related by a constant or order unity, determined by the relative strength of the two microwave field couplings (in the example in Fig. 6, the constant is  $2\Omega_{13}^2\Omega_{23}^2/\Omega^4 = 0.5$ ). A glance at Fig. 6(b) reveals how choosing the observation time  $t \sim \gamma_{12}^{-1}$  will give the best sensitivity in the measurement.

The inset of Fig. 6(b) shows the prediction (17) in comparison with the analytic results and we see good agreement. The adiabatic elimination and the expansion for small  $\gamma_{12}$  require  $2\gamma_{12}\Gamma_3^{(t)}/\Omega^2 \ll 1$  and  $\gamma_{12} \ll \Gamma_3^{(t)}$ . This ratio is 0.07 for  $\gamma_{12} = (2\pi) 5$  MHz. For higher dephasing rates, the dephasing rate competes with the preparation rate, and the first order expansion in  $\gamma_{12}$  becomes less valid. Such a case is seen in Fig. 6(a) (dashed, blue curve) where we plot  $\rho_{33}$  for a case with  $\gamma_{12} = (2\pi) 20$  MHz. The exponential decay occurs with a time scale comparable to the transient time to reach the quasi-steady state plateau. In such cases,  $\gamma_{12}$  can only be estimated from the tunneling rate by more detailed modeling of the underlying Bloch equations (15). We note that the microwave field intensity can be adjusted to control  $\Omega^2$  and to bring us into a regime where (17) is valid. The breakdown of this inequality occurred in the slow measurement time (25 ns) case plotted in Fig. 5(a,b), for which  $\Gamma_3^{(t)} \approx 4|\sigma_{34}|^2/\Gamma_4$  became quite large ( $\sim$  GHz).

When detuning and dephasing are both present but sufficiently small, the two effects add linearly. In Fig. 6(c) we show the population remaining versus detuning  $\Delta_{13}$ , with  $\gamma_{12} = (2\pi)1$  MHz (with  $\Delta_{23} = 0$ ) both in a strong field ( $2\gamma_{12}\Gamma_3^{(t)}/\Omega^2 = 0.016$ ) and weak field ( $2\gamma_{12}\Gamma_3^{(t)}/\Omega^2 = 0.18$ ) case. The prediction  $P = \exp(-(R_L^{(\gamma_{12})} + R_L^{(\Delta_2)})t)$  holds for the stronger field but overestimates the loss for the weaker field.

We conclude from the above calculations that there are two basic conditions that have to be satisfied for a reliable measurement of the decoherence in the system. First, the decoherence rate  $\gamma_{12}$  should be much smaller than the loss rate  $\Gamma_3^{(t)}$ , which holds in systems of interest. Second, we must be able to apply sufficiently strong fields that the preparation rate  $\Omega^2/\Gamma_3^{(t)}$  dominates  $\gamma_{12}$ .

### C. EIT with incoherent population loss and exchange

When the decoherence of  $\rho_{12}$  occurs due to population loss and exchange instead of dephasing, the effect on the EIT is much the same, with the  $\gamma_{12}$  simply replaced by the total decoherence rate. However, because these processes involve additional changes in the populations, the population loss rate, which we use to diagnose the decoherence rate, will be different.

Referring back to evolution matrix (16), we again find the eigenvalues to determine the loss

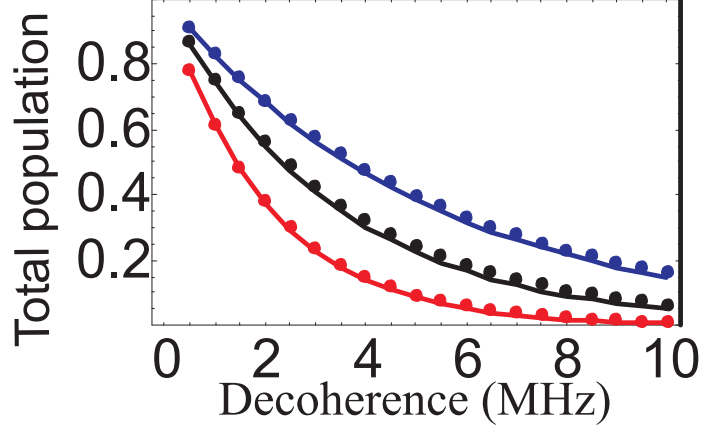


FIG. 7: (Color online) **EIT loss with dephasing, open loss, and closed loss** The population loss after 100 ns for several types of decoherence. The parameters are as in Fig. 6(c) but with  $\Omega_{23} = (2\pi)150$  MHz. The curves show the analytic predictions (17) and (18) and the dots show numerical results. The lowest curve is for purely open loss  $\Gamma_2^{(t)}$ , the middle curve for pure dephasing  $\gamma_{12}$ , and the top curve shows pure population exchange  $\Gamma_{2 \rightarrow 1}$ . The horizontal axis shows the corresponding decoherence rate for each case:  $\Gamma_2^{(t)}/2$ ,  $\gamma_{12}$ ,  $\Gamma_{2 \rightarrow 1}/2$ , respectively.

rate of the dark state. Expanding to first order in  $\Gamma_1^{(t)}$ ,  $\Gamma_2^{(t)}$ ,  $\Gamma_{2 \rightarrow 1}$ , respectively, we find:

$$\begin{aligned} R_L^{(\Gamma_1^{(t)})} &= \Gamma_1^{(t)} \frac{|\Omega_{23}|^2}{\Omega^2}; \\ R_L^{(\Gamma_2^{(t)})} &= \Gamma_2^{(t)} \frac{|\Omega_{13}|^2}{\Omega^2}; \\ R_L^{(\Gamma_{2 \rightarrow 1})} &= \Gamma_{2 \rightarrow 1} \frac{|\Omega_{13}|^4}{\Omega^4} \end{aligned} \quad (18)$$

It is interesting to note that the coefficient will depend in different ways on the relative intensities of the two fields depending on the origin of the decoherence. Fig. 7 shows the population loss after 100 ns for different kinds of loss, each plotted versus the total decoherence rate of  $\rho_{12}$ . The open system loss  $\Gamma_2^{(t)}$  is greater than the pure dephasing case because there is direct population loss on top of the absorption into  $\rho_{33}$  due to decay out of the dark state. The closed system loss (intrawell relaxation  $\Gamma_{2 \leftarrow 1}$ ) is seen to be smaller than pure dephasing, however, (18) shows that this could be greater or smaller depending on the relative values of  $\Omega_{13}$  and  $\Omega_{23}$ .

While we assumed in this discussion that the intra-well relaxation of  $|3\rangle$  was negligible ( $\Gamma_{3 \rightarrow 1} + \Gamma_{3 \rightarrow 2} \ll \Gamma_3^{(t)}$ ), the present discussion is easily generalized when this can not be assumed. In this case the population loss rate is the same as before, multiplied by a factor reflecting the proportion

of atoms in  $|3\rangle$  which actually tunnels to the right well:  $\Gamma_3^{(t)}/(\Gamma_{3\rightarrow 1} + \Gamma_{3\rightarrow 2})$ . This reflects the fact that excitation of  $|3\rangle$  due to decoherence will only be registered as population loss upon tunneling to the right well.

#### D. Resonant tunneling loss out of left well

Just as the decay of  $|3\rangle$  is the result of tunneling followed by decay of  $|4\rangle$ , interwell tunneling of  $|2\rangle$ , which is conceivably a leading order effect in the decoherence, involves tunneling to a near resonant level  $|5\rangle$  (see Fig. 1(c)). Here we consider this effect in detail to find the conditions where an effective damping rate  $\Gamma_2^{(t)}$  can be used, and also explore conditions where the dynamics are more complicated.

To explore this issue, we have performed numerical simulations for the system  $\{|1\rangle, |2\rangle, |3\rangle, |5\rangle\}$  where level  $|2\rangle$  is detuned from  $|5\rangle$  by  $\delta_{25} \equiv \omega_5 - \omega_2$ . The Hamiltonian (with the transformation  $\delta_5 = \Delta_2 + \delta_{25}$ ) is:

$$\mathcal{H} = \frac{\hbar}{2} \begin{bmatrix} 0 & 0 & \Omega_{13}^* & 0 \\ 0 & -2\Delta_2 & \Omega_{23}^* & 2\sigma_{25} \\ \Omega_{13} & \Omega_{23} & -2\Delta_{13} - i\Gamma_3^{(t)} & 0 \\ 0 & 2\sigma_{25} & 0 & -i\Gamma_5 - 2(\Delta_2 + \delta_{25}) \end{bmatrix}, \quad (19)$$

Mathematically similar energy level structures have been considered in the context of atomic systems [47].

In the following we take  $\sigma_{25} = (2\pi)5$  MHz and set the pure dephasing  $\gamma_{12} = 0$  to isolate the contribution from the presently considered effect. Analogous to Section III D, when  $\Gamma_5 \gg \sigma_{25}$  one can easily reduce the system to an effective-three level system with an additional loss rate  $\Gamma_2^{(t)} = 4|\sigma_{25}|^2\Gamma_5/(\Gamma_5^2 + 4\delta_{25}^2)$ . The small (black) dots in Fig. 8(a) present the population as a function of the detuning  $\Delta_{13}$  (keeping  $\Delta_{23} = 0$ ) after 100 ns of evolution for a case with  $\Gamma_5^{-1} = 2$  ns  $\approx (15\sigma_{25})^{-1}$  (and  $\delta_{25} = 0$ ). The results are in good agreement with the prediction one obtains from the loss rate Eq. (18) with this predicted tunneling rate  $\Gamma_2^{(t)}$  (solid curve). Fig. 8(b) shows the computed loss (dots) for resonant fields ( $\Delta_{13} = 0$ ) compared with the loss expected from the calculated  $\Gamma_2^{(t)}$  (solid curve) as a function of  $\Gamma_5^{-1}$ , for two different field strengths. One sees the estimate is good for  $\Gamma_5^{-1} < 5$  ns. The inset shows  $\rho_{55}$  versus time when  $\Gamma_5^{-1} = 5$  ns. One sees it quickly reaches a quasi-steady state plateau, then undergoes an exponential decay.



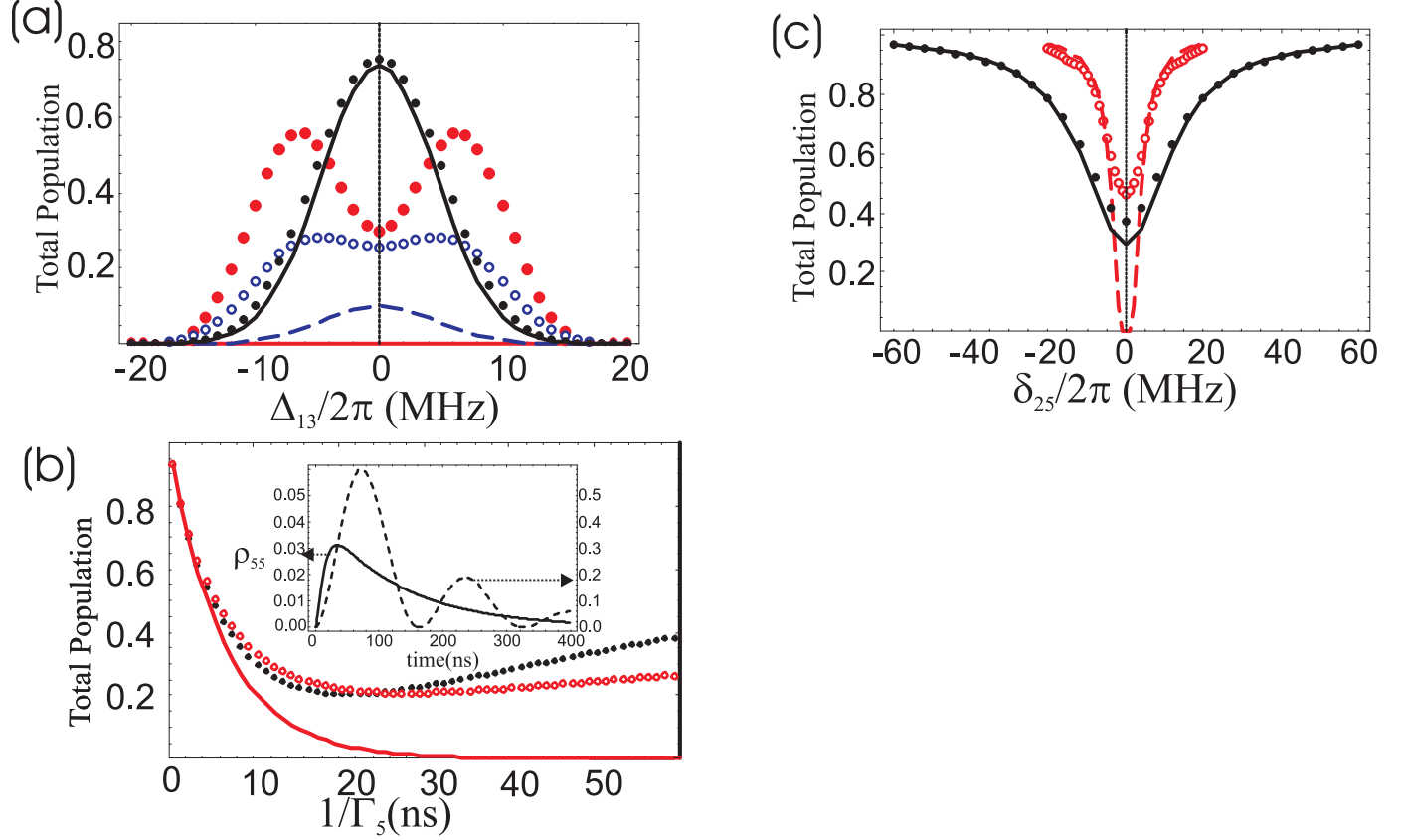


FIG. 8: (Color online) **Loss due to resonant tunneling to right well.** In the simulations we assume a (resonant) tunneling rate  $\sigma_{25} = (2\pi)5$  MHz, with fields  $\Omega_{13} = 0.8\Omega_{23}$  and the corresponding dark state  $\rho_{11} = 0.61$ ,  $\rho_{22} = 0.39$ ,  $\rho_{12} = -\sqrt{\rho_{11}\rho_{22}}$ . **(a)** The population remaining at 100 ns of fields applied with strength  $\Omega_{23} = 50$  MHz, versus the detuning  $\Delta_{13}$  (keeping  $\Delta_{23} = 0$ ), but varying the relaxation time  $\Gamma_5^{-1}$ . For the small solid dots (black)  $\Gamma_5^{-1} = 2$  ns. The solid curve shows the analytic prediction based on the effective loss rate  $\Gamma_2^{(t)}$  described in the text. The open (blue) dots show a case  $\Gamma_5^{-1} = 15$  ns, in which case a splitting appears in the resonance, contrary to the analytic prediction (dashed curve). The large (red) dots show the case  $\Gamma_5^{-1} = 80$  ns, for which the splitting becomes more pronounced and the loss rate quite small, while the  $\Gamma_2^{(t)}$  model predicts complete loss of the population. **(b)** The population remaining at 100 ns at the two photon resonance ( $\Delta_{13} = \Delta_{23} = 0$ ) versus  $\Gamma_5^{-1}$ . The solid (black) dots show the case  $\Omega_{13} = (2\pi)150$  MHz and the open (red) dots show  $\Omega_{13} = (2\pi)50$  MHz. They roughly agree with each other and the  $\Gamma_2^{(t)}$  model (solid curve) for  $\Gamma_5^{-1} \ll \sigma_{25}^{-1} = 32$  ns. However, for larger  $\Gamma_5^{-1}$  the loss becomes slower. The inset shows the population  $\rho_{55}$  for the a fast (5 ns, solid curve) and slow (80 ns, dashed) relaxation times  $\Gamma_5^{-1}$  (note the different scales). The fast case looks analogous to decoherence (see Fig. 6(a)), while oscillations occur in the slow case. **(c)** The population remaining versus the level detuning  $\delta_{25}$  in the case  $\Gamma_5^{-1} = 8$  ns (solid, black dots) and 80 ns (open, red dots). The solid and dashed curves show the  $\Gamma_2^{(t)}$  model predictions.

For larger  $\Gamma_5^{-1}$ , Fig. 8(b) shows the loss begins to decrease in contrast to the analytic estimate. The red curve in Fig. 8(a) shows the population remaining versus detuning  $\Delta_{13}$  in a case in for  $\Gamma_5^{-1} = 80$  ns. Besides the  $\Gamma_2^{(t)}$  model incorrectly predicting complete loss of the population after 100 ns, in the numerical results there is the clear appearance of double-peaked structure. This can be understood from the coupling  $\sigma_{25}$  giving rise to two eigenstates  $(|2\rangle \pm |5\rangle)/\sqrt{2}$  split by  $2\sigma_{25}$ , each of which gives rise to a distinct EIT resonance. The initial state (no population in  $|5\rangle$ ) is a superposition of these eigenstates and we get oscillations of the population between  $|2\rangle$  and  $|5\rangle$ . The inset in Fig. 8(b) (dashed curve) shows these oscillations in  $\rho_{55}$  for  $\Gamma_5^{-1} = 80$  ns. Because of the weak damping, the oscillations persist and the quasi-steady state is not reached during the time scale plotted. The dotted curve and open dots in Fig. 8(b) show an intermediate case  $\Gamma_5^{-1} = 15$  ns where the double peak structure is just becoming apparent, and the analytic estimate has begun to break down.

In Fig. 8(c) we address the case where the tunneling levels  $|2\rangle$  and  $|5\rangle$  can be slightly off-resonant ( $\delta_{25} \neq 0$ ). The filled dots show the population remaining for  $\Gamma_5^{-1} = 8$  ns versus  $\delta_{25}$ . The solid curve shows the  $\Gamma_2^{(t)}$  model estimate, which correctly accounts for the slower tunneling rate as we move off resonance. The red dots show the same for  $\Gamma_5^{-1} = 80$  ns. In this limit, the analytic estimate expression severely overestimates the loss for  $\delta_{25} < \Gamma_5$  but as we move off resonance, the coherent tunneling plays less of a role and the effective tunneling decay rate model becomes more accurate.

In summary, tunneling of our lower states will be a source of loss in EIT. The behavior will depend qualitatively on the relative strength of the coherent coupling and the loss rate of the additional quantum level and so can provide us with information about these quantities. In the limit where the loss rate dominates, we see how it reduces to an open system loss of  $|2\rangle$  where as in the other limit we see a qualitative signature (the splitting of the resonance) of coherent coupling to another level.

## V. EIT WITH RADIATION CROSS-TALK

To now, we have considered how EIT is affected by decoherence and tunneling to other levels. Another important consideration to include is that all levels are dipole coupled and so in principle coupled by the microwave fields. The RWA allows us to neglect the majority of the couplings as the dynamics are dominated by couplings which are near resonant. For example, one need not

consider the coupling of field  $b$  on the  $|1\rangle \leftrightarrow |3\rangle$  transition or field  $a$  on  $|2\rangle \leftrightarrow |3\rangle$ . However, in SQCs, the relative scale of the Rabi frequencies ( $\sim 100$  MHz) to the level spacings ( $\sim$  GHz) is somewhat larger than in typical atomic systems. Thus, it is important to know the magnitude and type of effects that these “cross” couplings can have. Here we consider, separately, a case with cross coupling within the three level system, and a case where fields couple to an additional excited level. In general, we find these effects can be characterized analytically in terms of additional loss rates and AC Stark shifts. If one neglected these effects, there are configurations where one may mistakenly attribute a loss rate to a dephasing when in fact it is due to off-resonant field coupling. While we found it was beneficial to turn the microwave coupling strengths  $\Omega^2$  up to overcome decoherence and detuning, we will see how this can increase the importance of these cross-talk effects. We will also see how proper understanding of the effects can allow us to mitigate them by properly compensating for the Stark shifts. To isolate these cross-talk effects, we will set other losses and dephasings to zero in the following.

#### A. Radiation cross-talk in a three-level system

In the configuration proposed here and in [19], the qubit states  $|1\rangle$  and  $|2\rangle$  are the first two levels of a slightly anharmonic potential (the left well), while the excited level  $|3\rangle$  is the third such level. Therefore, the level spacing  $\omega_3 - \omega_2$  is only slightly different than  $\omega_2 - \omega_1$  (with the parameters proposed the spacings are  $\sim 30$  GHz and the difference is 0.7 GHz). As a result, the field  $\Omega_{23}$  is only 0.7 GHz detuned from  $|1\rangle \leftrightarrow |2\rangle$  (see Fig. 9(a)). A rough estimate of this effect was noted in [19]. Here we present an analytic treatment which shows it causes an AC Stark shift which depends on the relative dipole coupling strengths, field intensities, and level spacings. Thus the EIT resonance position can be a function of field amplitudes used, which can be compensated by adjusting the field frequencies.

We consider the Hamiltonian (9) but do not invoke the RWA with respect to terms rotating by the mismatch frequency between the  $|2\rangle \leftrightarrow |3\rangle$  and  $|1\rangle \leftrightarrow |2\rangle$  transitions  $\delta \equiv (\omega_2 - \omega_1) - (\omega_3 - \omega_2)$ .

$$\mathcal{H} = \frac{\hbar}{2} \begin{bmatrix} 0 & \beta^* \Omega_{23}^* e^{i\delta t} & \Omega_{13}^* \\ \beta \Omega_{23} e^{-i\delta t} & -2\Delta_2 & \Omega_{23}^* \\ \Omega_{13} & \Omega_{23} & -2\Delta_{13} - i\Gamma_3^{(t)} \end{bmatrix}, \quad (20)$$

where  $\beta \equiv x_{12}/x_{23}$  is the ratio of dipole moments between the additional off-resonant transition

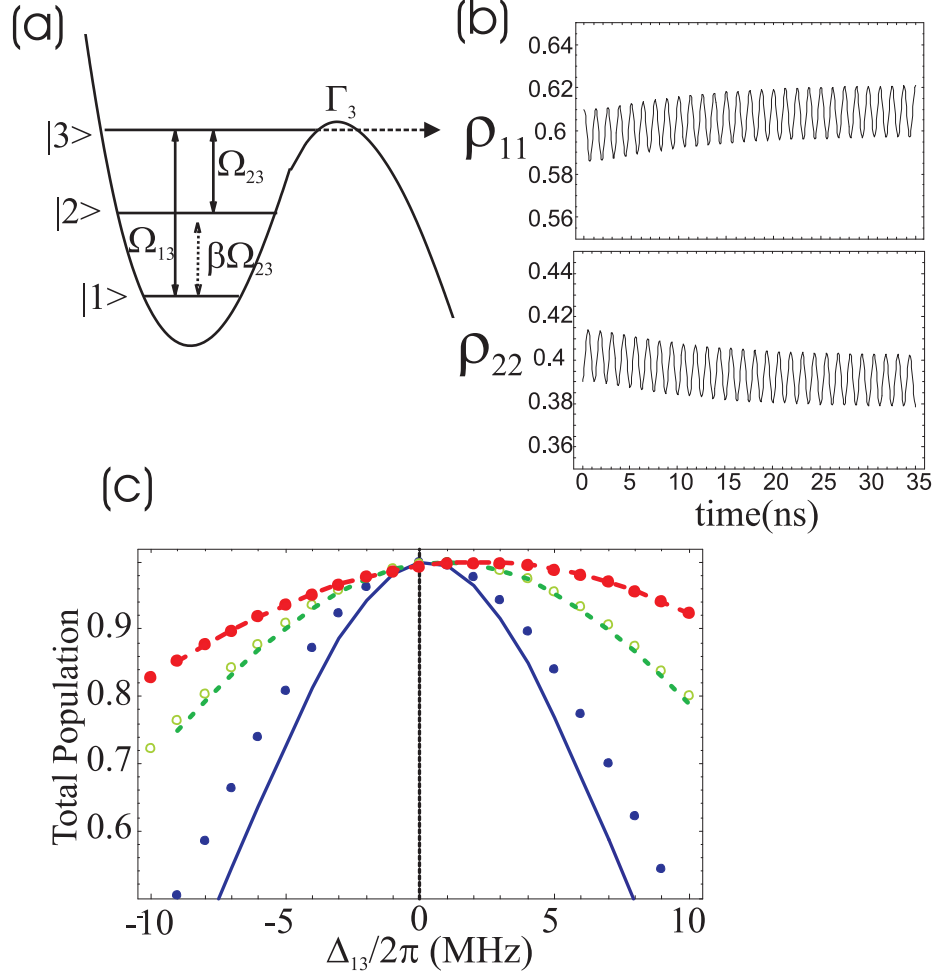


FIG. 9: (Color online) **Cross talk in a ladder system.** (a) Schematic of the dominant cross-talk term: field  $b$  (resonant with  $|2\rangle \leftrightarrow |3\rangle$ ) also couples  $|1\rangle \leftrightarrow |2\rangle$ , detuned by 0.7 GHz. (b) This induces fast oscillations of the ground state populations  $\rho_{11}$  and  $\rho_{22}$  (and a slow overall drift) as shown here for the initial state  $\rho_{11} = 0.61$ ,  $\rho_{22} = 0.39$  with full coherence and  $\Omega_{13} = 0.8 \Omega_{23} = (2\pi)120$  MHz and  $\Gamma_3^{(t)} = (2\pi)159$  MHz. (c) Population remaining at 50 ns for  $\Omega_{23} = (2\pi)50$  MHz (small, blue dots), 100 MHz (open, green dots), and 150 MHz (large, red dots), with the curves showing the analytic predictions based on the AC Stark shifts described in the text.

and the intended resonant transition for the field  $b$ . In the case we are considering  $\beta = -2.55$  though it should be emphasized that these ratios are strong functions of the parameters and can vary by an order of magnitude.

We performed a numerical propagation of the density matrix equations (8) for this Hamiltonian for the resonant case  $\Delta_{13} = \Delta_{23} = 0$  and plot the evolution of  $\rho_{11}$  and  $\rho_{22}$  in Fig. 9(b). We see the

extra coupling gives rise to a small amplitude, rapid oscillations of both quantities. Considering a toy two-level model with only the off-resonant coupling present predicts population oscillations of period  $(2\pi)/\delta$  and amplitude  $\sim |\beta\Omega_{23}|/2\delta$ , in agreement with the numerical results. The small deviations of  $\rho_{11}, \rho_{22}$  from their dark state values gives rise to absorption into  $|3\rangle$  and thus loss. In the toy model, an off-resonant coupling can be accounted for as an AC Stark shift. In particular,  $\omega_1$  and  $\omega_2$  are predicted to shift by  $\pm \sim |\beta\Omega_{23}|^2/4\delta$ , respectively. This results in an effective shift of the two-photon detuning  $\Delta_2$  which can be compensated.

Stated in terms of our exponential loss language, the loss rate  $R_L^{(\Delta_2)}$  (13) is still valid but the two-photon detuning  $\Delta_2$  should be replaced by  $\Delta_2 + \Delta_{AC}^{(12)}$ , where

$$\Delta_{AC}^{(12)} = \frac{|\beta\Omega_{23}|^2}{2\delta} \quad (21)$$

In Fig. 9(c) we plot the population remaining versus  $\Delta_{13}$  (keeping  $\Delta_{23} = 0$ ) for three different values of field intensities. The solid curves show the theoretical prediction based on the predicted AC Stark shift. They are in good agreement (the overestimate of loss at the lowest intensities with some detuning is due to the damping of the absorbing that being too weak to efficiently keep the SQC in the dark state). Importantly, if one adjusts the field frequencies, one can completely avoid loss due to the cross-talk coupling. Strictly speaking, there is a small loss if  $|2\rangle$  decays at some small rate  $\Gamma_2^{(t)}$ , however, this loss is much smaller than the loss already predicted from the associated decoherence (18).

## B. Effect of off-resonant radiation coupling to an additional excited level

The last important situation we consider is that of coupling to an additional excited level  $|e\rangle$ , coupled off-resonantly to states  $|1\rangle$  and  $|2\rangle$  via the two applied fields  $a$  and  $b$ , thus forming a “double- $\Lambda$ ” system [48], as diagrammed in Fig. 10(a). As we will see, the extra coupling gives rise to AC Stark shifts in much the same way as we saw in Section V A. In addition, because  $|e\rangle$  (unlike  $|2\rangle$ ) is quickly decaying, the coupling gives rise to some population loss even when the AC Stark shift is compensated.

Dropping the RWA with respect to terms coupling to level  $|e\rangle$  and defining  $\delta_{3e} \equiv \omega_e - \omega_3$ , the Hamiltonian (using a frame  $\delta_e = \Delta_{13} + \delta_{3e}$ ) is

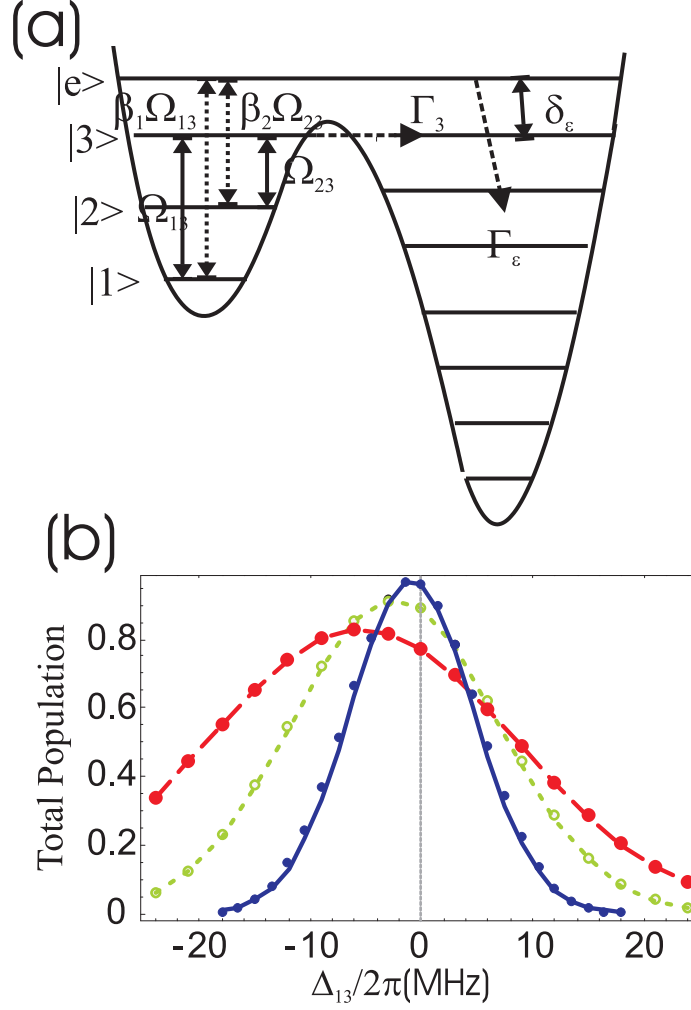


FIG. 10: (Color online) **Coupling to an additional excited level.** (a) Schematic of off-resonant microwave coupling of each of states  $|1\rangle$  and  $|2\rangle$  to an additional level  $|e\rangle$  above the barrier. (b) The population remaining at 100 ns for the same initial state and relative field strengths as in Fig. 9. We show the cases  $\Omega_{23} = (2\pi)60$  MHz (small solid, blue), 100 MHz (open, green), and 150 MHz (large solid, red). The solid curves show the loss and AC Stark shift predicted in the text (25). To isolate and clearly show the effect we have set  $\beta = 0$  (from (20)) and used  $\delta_{3e} = (2\pi)1.5$  GHz, instead of the  $(2\pi)10$  GHz we predict for our proposed parameters. We use  $x_{14} = 0.0054$  and  $x_{24} = -0.0437$  and  $\Gamma_e = \Gamma_3^{(t)} = (2\pi)159$  MHz.

$$\mathcal{H} = \frac{\hbar}{2} \begin{bmatrix} 0 & 0 & \Omega_{13}^* & \beta_1^* \Omega_{13}^* \\ 0 & -2\Delta_2 & \Omega_{23}^* & \beta_2^* \Omega_{23}^* \\ \Omega_{13} & \Omega_{23} & -2\Delta_{13} - i\Gamma_3^{(t)} & 0 \\ \beta_1 \Omega_{13} & \beta_2 \Omega_{23} & 0 & -2(\Delta_{13} + \delta_{3e}) - i\Gamma_e \end{bmatrix}, \quad (22)$$

with  $\beta_i \equiv x_{i4}/x_{i3}$ . We have assumed some large open loss channel  $\Gamma_e$ .

In the case where only one of the couplings is present ( $\beta_1 = 0$  or  $\beta_2 = 0$ ), the effect is simple to calculate. When  $\beta_1 = 0$ , one can consider the Schrödinger evolution  $\dot{c}_e$  from Eq. (22) and adiabatically eliminate  $c_e$  to obtain

$$c_e = -i \frac{\beta_2 \Omega_{23} c_2}{2i\delta_{3e} - \Gamma_e} \quad (23)$$

where we have assumed  $\delta_{3e} \gg \Delta_{13}$ . Substituting this back into the equation for  $\dot{c}_2$  yields:

$$\dot{c}_2 = -\frac{i}{2} \Omega_{23} c_3 - i\Delta_2 c_2 - |\beta_2 \Omega_{23}|^2 \left( \frac{2i\delta_{3e} + \Gamma_e}{8\delta_{3e}^2 + 2\Gamma_e^2} \right) c_2 \quad (24)$$

revealing that the extra coupling gives rise to a Stark shift and population decay of  $|2\rangle$ . In the large detuning limit ( $\delta_{3e} \gg \Gamma_e$ ), the Stark shift is  $|\beta_2 \Omega_{23}|^2 / 4\delta_{3e}$  and we have an effective loss rate from  $|2\rangle$ ,  $\Gamma_2^{(e)} = |\beta_2 \Omega_{23}|^2 \Gamma_e / 4\delta_{3e}^2$ . Analogous results occur when  $\beta_2 = 0$ , leading to a Stark shift of the two-photon resonance of opposite sign. The population loss rates will in turn contribute to the decoherence and cause exponential loss from the EIT as discussed in Section IV.

When both are present, the shifts and loss rates are not simply the sum of the two separate contribution, due to interferences between them. A case where summing the two contributions clearly does not work is  $\beta_1 = \beta_2$  (equal dipole ratios). In this case (and *only* this case) the dark state  $c_2/c_1 = -\Omega_{13}/\Omega_{23}$  is also completely decoupled from  $|4\rangle$ . Thus no population loss or Stark shift is induced in this case. To obtain an expression in the general case, we follow the following procedure. We adiabatically eliminate  $c_3$  and  $c_e$  from the Schrödinger equation from Eq. (22), obtain the  $2 \times 2$  evolution matrix for  $c_1$  and  $c_2$ , then solve for the eigenvalues of this matrix. One of the values has a large imaginary part (which reduced to  $\Omega^2/\Gamma_3^{(t)}$  in the limit  $\beta_1 = \beta_2 = 0$ ) and corresponds to the absorbing state. The other has a small imaginary part which vanishes when  $\beta_1 = \beta_2 = 0$  and corresponds to the dark state. We investigated the imaginary part of this eigenvalue in the limit that  $\Omega^2/\Gamma_3^{(t)} \gg \Delta_{13}, \Delta_{23}$  and  $\beta_i \Gamma_e / \delta_{3e} \ll 1$  and then minimized this

expression with respect to the two-photon detuning  $\Delta_2$  (when  $\Delta_{23} = 0$ ) to obtain the Stark shift. The loss rate and shift of the resonance obtained were:

$$\begin{aligned} R_L^{(e)} &= \frac{|\Omega_{13}|^2 |\Omega_{23}|^2}{\Omega^4} \frac{\Omega^2 \Gamma_e}{4\delta_{3e}^2 + \Gamma_e^2} |\beta_1 - \beta_2|^2; \\ \Delta_{AC}^{(e)} &= -\frac{\delta_{3e}}{4\delta_{3e}^2 + \Gamma_e^2} (\beta_1 - \beta_2) (\beta_1 |\Omega_{13}|^2 + \beta_2 |\Omega_{23}|^2). \end{aligned} \quad (25)$$

These expressions reduce to the simpler cases above ( $\beta_1 = 0$  or  $\beta_2 = 0$ ) and also disappear when  $\beta_1 = \beta_2$ . Interestingly, the relative sign of the dipole moments plays an important role. For example if  $\beta_1 = -\beta_2$  the loss rate is actually twice what one would expect from the sum of the individual couplings. In this case, the dark state  $\Psi_D$  for  $|3\rangle$  is actually the absorbing state for  $|4\rangle$ .

In Fig. 10(b) we plot the population remaining versus detuning  $\Delta_{13}$  for three different field intensities in the system we have been considering, but now considering the coupling to the additional level  $|e\rangle$ . The dots show numerical propagation of the density matrix equations corresponding to Eq. (22). Note that to isolate the effect studied at present, we have ignored the cross-talk considered in Section V A (by setting  $x_{12} = 0$ ) and set the pure dephasing  $\gamma_{12} = 0$ . The solid curves then show the analytic estimate based on the Stark shifts and loss rates (25). One sees excellent agreement.

It should be noted that this analysis should be able to account for the effect of multiple excited levels  $e_j$  by simply summing their contributions  $\sum_j R_L^{(e_j)}$  and  $\sum_j \Delta_{AC}^{(e_j)}$ . Because of the large frequency differences between each successive level, coherent interference between contributions from different  $|e_j\rangle$  will not occur.

## VI. CONCLUSION

We have described in detail a proposal for demonstrating a quantum optical effect, EIT, in a SQC. In this context, EIT will manifest itself as the suppression of photon-induced tunneling from stable states  $|1\rangle, |2\rangle$  through some read-out state  $|3\rangle$ , due to quantum mechanical interference for two paths of excitation. This provides a method of unambiguously demonstrating phase coherence in these systems. We have provided a thorough and mostly analytic treatment of EIT in the presence of complicating effects due to decoherence and multiple levels in SQCs, which will be important in guiding experimental implementation and observation of EIT and other quantum interference effects.



We analyzed in detail first the basic considerations of EIT such as imperfect dark state preparation, and one- and two-photon detuning and determined the expected experimental signatures. Under appropriate conditions, we obtained an expression for the total population as a function of time Eq. (11), which describes a fast loss of the absorbing component, followed by a small exponential loss of the system. Over shorter times, EIT thus provides a method to confirm the successful preparation (and coherence) of the particular dark state defined by the microwave fields applied. For longer times, the observed loss rate will be function of both the detuning from two-photon resonance as well as decoherence effects. We also discussed the important issue of how the measurement state  $|4\rangle$  plays a role in the decay of the read-out state  $|3\rangle$  and saw how the biasing condition of these levels and the SQUID measurement rate can have a large effect on the parameters of the effective three-level system.

We then discussed in detail how decoherence due to dephasing of the qubit coherence, incoherent population loss or exchange, and tunneling of levels through the barrier effects the loss rate. Measuring these loss rates can then be a powerful tool which sensitively probes these various processes. We obtained the coefficients for the loss rates, which depend differently on the field strengths, depending on the underlying decoherence processes. For the case of primarily coherent resonant tunneling, we found that that the EIT will exhibit a qualitatively different double-peaked structure. Probing these effects with EIT can aid in understanding and minimizing decoherence and give information about the full multi-level structure of the SQC. A potentially interesting future investigation is to learn the signature from coupling to other quantum degrees of freedom, such as the microresonators postulated in [27].

Finally we have found that the microwave fields themselves can cause additional loss rates and AC Stark shifts of the EIT resonance which must be accounted for when one uses stronger field strengths. Importantly, we found that, these effects can become more pronounced with  $\Omega^2$ , meaning there will be some intermediate field strength which balances these considerations with the decoherence and detuning effects. Also, we showed how these effects could be mitigated by proper compensation of the Stark shifts.

This work was supported in part by the AFOSR grant No. F49620-01-1-0457 under the Department of Defense University Research Initiative in Nanotechnology (DURINT). The work at Lincoln Laboratory was sponsored by the AFOSR under Air Force Contract No. F19628-00-C-

0002. Z.D. acknowledges support from the Office of Naval Research.

---

- [1] A. J. Leggett and A. Garg, Phys. Rev. Lett. **54**, 857 (1985).
- [2] J. R. Friedman, V. Patel, W. Chen, S. K. Tolpygo and J. E. Lukens, Nature (London) **406**, 43 (2000).
- [3] C. H. van der Wal, A. C. J. ter Haar, F. K. Wilhelm, R. N. Schouten, C. J. P. M. Harmans, T. P. Orlando, S. Lloyd, and J. E. Mooij, Science **290**, 773 (2000).
- [4] A. J. Berkley, H. Xu, R. C. Ramos, M. A. Gubrud, F. W. Strauch, P. R. Johnson, J. R. Anderson, A. J. Dragt, C. J. Lobb, F. C. Wellstood, Science **300**, 1548 (2003).
- [5] H. Xu, F. W. Strauch, S. K. Dutta, P. R. Johnson, R. C. Ramos, A. J. Berkley, H. Paik, J. R. Anderson, A. J. Dragt, C. J. Lobb, F. C. Wellstood, Phys. Rev. Lett. **94**, 027003 (2005).
- [6] Y. Nakamura, Y. A. Pashkin, and J. S. Tsai, Nature (London) **398**, 786 (1999); Yu. A. Pashkin, T. Yamamoto, O. Astafiev, Y. Nakamura, D. V. Averin and J. S. Tsai, *ibid.* **421**, 823 (2003).
- [7] Y. Nakamura, Y. A. Pashkin, J. S. Tsai, Phys. Rev. Lett. **87**, 246601 (2001).
- [8] D. Vion, A. Aassime, A. Cottet, P. Joyez, H. Pothier, C. Urbina, D. Esteve, and M. H. Devoret, Science **296**, 886 (2002).
- [9] Y. Yu, Y. Yu, S. Han, X. Chu, S.-I Chu, and Z. Wang, Science **296**, 889 (2002).
- [10] J. M. Martinis, S. Nam, J. Aumentado, and C. Urbina, Phys. Rev. Lett. **89**, 117901 (2002).
- [11] I. Chiorescu, Y. Nakamura, C. J. P. M. Harmans, and J. E. Mooij, Science **299**, 1869 (2003).
- [12] J. Claudon, F. Balestro, F. W. J. Hekking, O. Buisson, Phys. Rev. Lett. **93**, 187003 (2004).
- [13] I. Chiorescu, P. Bertet, K. Semba, Y. Nakamura, C.J.P.M. Harmans, and J.E. Mooij, Nature (London) **431**, 159 (2004).
- [14] A. Wallraff, D. I. Schuster, A. Blais, L. Frunzio, R.-S. Huang, J. Majer, S. Kumar, S. M. Girvin and R. J. Schoelkopf, Nature (London) **431**, 162 (2004).
- [15] W. D. Oliver, Y. Yu, J. C. Lee, K. K. Berggren, L. S. Levitov, and T. P. Orlando, Science **310** 1653 (2005); published online 10 November 2005, 10.1126/science.1119678.
- [16] M. Sillanpaa, T. Lehtinen, A. Paila, Yu. Makhlin, and P. Hakonen, cond-mat/0510559.
- [17] K. J. Boller, A. Imamoglu, and S. E. Harris, Phys. Rev. Lett. **66**, 2593 (1991).
- [18] S. E. Harris, Physics Today **50**, 36 (1997).
- [19] K. V. R. M. Murali, Z. Dutton, W. D. Oliver, D. S. Crankshaw and T. P. Orlando, Phys. Rev. Lett. **93**, 087003 (2004).

- [20] L. V. Hau, S. E. Harris, Z. Dutton, and C. H. Behroozi, *Nature (London)* **397**, 594 (1999); M. M. Kash, V. A. Sautenkov, A. S. Zibrov, L. Hollberg, G. R. Welch, M. D. Lukin, Y. Rostovtsev, E. S. Fry, and M. O. Scully, *Phys. Rev. Lett.* **82** 5229 (1999); D. Budker, D. F. Kimball, S. M. Rochester, and V. V. Yashchuk, *Phys. Rev. Lett.* **83**, 1767 (1999).
- [21] C. Liu, Z. Dutton, C. H. Behroozi and L. V. Hau, *Nature (London)* **409**, 490 (2001); D. F. Phillips, A. Fleischhauer, A. Mair, R. L. Walsworth and M. D. Lukin, *Phys. Rev. Lett.* **86**, 783 (2001).
- [22] M. Fleischhauer and M. D. Lukin, *Phys. Rev. Lett.* **84**, 5094 (2000).
- [23] C. H. van der Wal, M. D. Eisaman, A. Andr, R. L. Walsworth, D. F. Phillips, A. S. Zibrov, and M. D. Lukin *Science* **301** 196 (2003); A. Kuzmich, W. P. Bowen, A. D. Boozer, A. Boca, C. W. Chou, L.-M. Duan and H. J. Kimble, *Nature (London)* **423**, 731 (2003).
- [24] S. E. Harris and L. V. Hau, *Phys. Rev. Lett.* **82**, 4611 (1999); M. D. Lukin and A. Imamoglu, *Nature (London)* **413**, 273 (2001).
- [25] J. Ruostekoski and D. F. Walls, *Phys. Rev. A*, **59** R2571 (1999).
- [26] Y. Nakamura, Yu. A. Pashkin, T. Yamamoto, and J. S. Tsai, *Phys. Rev. Lett.* **88**, 047901 (2002).
- [27] R. W. Simmonds, K. M. Lang, D. A. Hite, S. Nam, D. P. Pappas, and J. M. Martinis, *Phys. Rev. Lett.* **93** 077003 (2004); K. B. Cooper, M. Steffen, R. McDermott, R. W. Simmonds, S. Oh, D. A. Hite, D. P. Pappas, and J. M. Martinis, *ibid.* **93**, 180401 (2004).
- [28] Z. Zhou, S.-I. Chu and S. Han, *Phys. Rev. B* **66**, 054527 (2002); C.-P. Yang, S.-I. Chu and S. Han, *Phys. Rev. A* **67**, 042311 (2003).
- [29] M. H. S. Amin, A. Yu. Smirnov, and A.M. van den Brink, *Phys. Rev. B* **67**, 100508(R) (2003).
- [30] E. Paspalakis and N. J. Klystra, *J. of Modern Optics* **51**, 1679 (2004); Z. Kis and E. Paspalakis, *Phys. Rev. B* **69**, 024510, (2004).
- [31] P.R. Johnson, W. T. Parsons, F. W. Strauch, J. R. Anderson, A. J. Dragt, C. J. Lobb, and F. C. Wellstood, *Phys. Rev. Lett.* **93** 187004 (2005).
- [32] N. Aravantinos-Zafiris and E. Paspalakis, *Phys. Rev. A* **72** 014303 (2005).
- [33] L.-C. Ku and C.C. Yu, *Phys. Rev. B* **72** 024526 (2005).
- [34] Y.-X. Liu, J. Q. You, L. F. Wei, C. P. Sun, F. Nori, *Phys. Rev. Lett.* **95**, 087001 (2005).
- [35] J. E. Mooij, T. P. Orlando, L. Levitov, L. Tian, C. H. van der Wal, and S. Lloyd, *Science* **285**, 1036 (1999).
- [36] T. P. Orlando, J. E. Mooij, L. Tian, C. H. van der Wal, L. S. Levitov, S. Lloyd, J. J. Mazo, *Phys. Rev. B* **60**, 15398 (1999).

- [37] A. T. Sornborger, A. N. Cleland, and M. R. Geller, Phys. Rev. A **70** 052315 (2004).
- [38] K. Segall, D. Crankshaw, D. Nakada, T. P. Orlando, L. S. Levitov, S. Lloyd, N. Markovic, S. O. Valenzuela, M. Tinkham, K. K. Berggren, Phys. Rev. B **67**, 220506(R) (2003).
- [39] D. S. Crankshaw, K. Segall, D. Nakada, and T. P. Orlando, L. S. Levitov, S. Lloyd, S. O. Valenzuela, N. Markovic, and M. Tinkham, K. K. Berggren, Phys. Rev. B., **69**, 144518 (2004).
- [40] Y. Yu, D. Nakada, J. C. Lee, B. Singh, D. S. Crankshaw, T. P. Orlando, K. K. Berggren, W. D. Oliver, Phys. Rev. Lett., **92**, 117904 (2004).
- [41] Y. Yu, W. D. Oliver, J. C. Lee, K. K. Berggren, L. S. Levitov, and T. P. Orlando, cond-mat/0508587.
- [42] M.O. Scully, M.S. Zubairy, *Quantum Optics*, (Cambridge Univ. Press, Cambridge, UK, 1997).
- [43] Z. Dutton, Ph.D. thesis (Harvard University, 2002).
- [44] W.H. Press, S.A. Teukolsky, W.T. Vetterling, and B.P. Flannery, *Numerical Recipes in C, 2nd Ed.* (Cambridge University Press, Cambridge, 1992).
- [45] J. Javanainen and J. Ruostekoski, Phys. Rev. A **52** 3033 (1995).
- [46] G. Burkard, R. H. Koch, and D. P. DiVincenzo, Phys. Rev. B., **69**, 064503 (2003).
- [47] M. D. Lukin, S. F. Yelin, M. Fleischhauer, and M. O. Scully, Phys. Rev. A **60**, 003225 (1999).
- [48] F.-L. Li and S.-Y. Zhu, Phys. Rev. A **59** 2330 (1999).